

**DEVELOPMENT OF METHODS AND TOOLS FOR ON-THE-FLY
RESPONSE FUNCTION GENERATION FOR CRITICALITY
CALCULATIONS**

A Dissertation
Presented to
The Academic Faculty

by

Ryan Paul Hon

In Partial Fulfillment
of the Requirements for the Degree
Doctor of Philosophy in the
School of Nuclear and Radiological Engineering

Georgia Institute of Technology
May 2016

COPYRIGHT© 2016 BY RYAN PAUL HON

**DEVELOPMENT OF METHODS AND TOOLS FOR ON-THE-FLY
RESPONSE FUNCTION GENERATION FOR CRITICALITY
CALCULATIONS**

Approved by:

Dr. Farzad Rahnema, Advisor
George W. Woodruff School
Georgia Institute of Technology

Dr. Bojan Petrovic
George W. Woodruff School
Georgia Institute of Technology

Dr. Dingkang Zhang
George W. Woodruff School
Georgia Institute of Technology

Dr. Edmond Chow
School of Computational Science and
Engineering
Georgia Institute of Technology

Dr. Alireza Haghightat
Department of Mechanical Engineering
*Virginia Polytechnic and State
University*

Dr. Luiz Leal
*Institut de Radioprotection et de Sûreté
Nucléaire (IRSN)*

Date Approved: March 31, 2015

Zu meiner Frau

ACKNOWLEDGEMENTS

I would like to thank everyone who has helped me to reach this milestone in my life and allowed me to develop into the man I am today. Although there are too many people to mention by name, I sincerely thank all of you for being a part of my life. I would especially like to thank my wife Kelly whose understanding and support have been essential during this long journey.

On the technical side, I would like to thank my advisor Dr. Farzad Rahnema who influenced me when I was an undergrad, led me to pursue graduate degrees, and ultimately supported me throughout my time at Georgia Tech. My appreciation also goes to the rest of my committee members for their service and advice. I am grateful to all of my teachers throughout the years whose lessons have prepared me to reach this point. Thanks also to all of my compatriots in the CRMP laboratory, who made my many years at Georgia Tech both enriching and entertaining.

Lastly, I would like to acknowledge that this work was accomplished under the support of an Integrated University Program Graduate Fellowship.

TABLE OF CONTENTS

	Page
ACKNOWLEDGEMENTS	iv
LIST OF TABLES	vii
LIST OF FIGURES	ix
SUMMARY	x
 <u>CHAPTER</u>	
1 INTRODUCTION	1
1.1 Motivation	2
1.2 Objectives	3
1.3 Organization	3
2 COMET METHODOLOGY	5
2.1 Response Generation	9
2.2 Deterministic Iteration Scheme	11
3 STOCHASTIC TRANSPORT METHODOLOGY	14
3.1 Mathematical Foundation for Stochastic Neutron Transport	14
3.2 Neutron Transport Implementation	18
3.2.1 Pseudo Random Number Generator	20
3.2.2 Geometry Specification	21
3.2.3 Sampling Distance to Collision	22
3.2.4 Determining Distances to Surfaces	23
3.2.5 Determining Whether a Collision Happens Within a Region	27
3.2.6 Sampling Collision Type	27
3.2.7 Multi-group Energy Formulation	28

3.2.8	Continuous Energy Formulation	31
3.2.9	Computing Responses	32
3.2.10	Variance Reduction	34
4	SPARC IMPLEMENTATION DETAILS	36
4.1	Response Generation Implementation	36
4.2	Database Management	38
4.3	Parallelization through the Message Passing Interface (MPI)	39
5	BENCHMARK RESULTS	45
5.1	Fixed Source Benchmarking	45
5.2	European Pressurized Reactor Benchmark	47
5.2.1	Assembly Specification	48
5.2.2	HELIOS Nuclear Data Generation	52
5.2.3	COMET Response Calculations	55
5.2.4	Uncontrolled Assembly Results	58
5.2.5	Controlled Assembly Results	61
5.2.6	Gadded Assembly Results	64
6	CONCLUSION	68
APPENDIX A:	ASSEMBLY LEVEL RESULTS	69
APPENDIX B:	MULTI-GROUP CROSS SECTIONS	72
REFERENCES		97
VITA		98

LIST OF TABLES

	Page
Table 1: Combinatorial geometry specifications for regions in Figure 2.	22
Table 2: Formulas for some simple geometries.	24
Table 3: Sampling collision type.	28
Table 4: Multi-group cross section definitions	29
Table 5: Time to solution for response function generation using different parallelization schemes.	42
Table 6: Fixed source benchmark results for escape, absorption, and fission for MCNP and SPaRC.	46
Table 7: Difference in fixed source benchmark results between MCNP and SPaRC.	47
Table 8: EPR geometric assembly parameters.	48
Table 9: EPR material compositions.	51
Table 10: EPR assembly temperatures.	51
Table 11: Energy group structure for cross section generation.	53
Table 12: Uncontrolled assembly coarse meshes.	55
Table 13: Controlled assembly coarse meshes.	55
Table 14: Gadded assembly coarse meshes.	55
Table 15: Difference between MCNP and SPaRC response functions for the fuel pin coarse mesh in the uncontrolled assembly case.	59
Table 16: Difference between MCNP and SPaRC response functions for the guide tube coarse mesh in the uncontrolled assembly case.	59
Table 17: COMET eigenvalue results and standard deviations for the uncontrolled EPR assembly with responses generated by both MCNP and SPaRC.	60
Table 18: Difference in COMET pin powers for the uncontrolled EPR assembly with responses generated with both MCNP and SPaRC.	60
Table 19: Difference between MCNP and SPaRC response functions for the fuel pin coarse mesh in the controlled assembly case.	62

Table 20: Difference between MCNP and SPaRC response functions for the control rod coarse mesh in the uncontrolled assembly case.	62
Table 21: COMET eigenvalue results and standard deviations for the controlled EPR assembly with responses generated by both MCNP and SPaRC.	63
Table 22: Difference in COMET pin powers for the controlled EPR assembly with responses generated with both MCNP and SPaRC.	63
Table 23: Difference between MCNP and SPaRC response functions for the fuel pin coarse mesh in the gadded assembly case.	65
Table 24: Difference between MCNP and SPaRC response functions for the guide tube coarse mesh in the gadded assembly case.	65
Table 25: Difference between MCNP and SPaRC response functions for the 2% gadolinium fuel pin coarse mesh in the gadded assembly case.	65
Table 26: Difference between MCNP and SPaRC response functions for the 8% gadolinium fuel pin coarse mesh in the gadded assembly case.	66
Table 27: COMET eigenvalue results and standard deviations for the gadded EPR assembly with responses generated by both MCNP and SPaRC.	66
Table 28: Difference in COMET pin powers for the gadded EPR assembly with responses generated with both MCNP and SPaRC.	67

LIST OF FIGURES

	Page
Figure 1: Spatial domain decomposition, the volume V is split into non-overlapping regions V_{ij} with boundary conditions dependent on adjacent volumes.	6
Figure 2: An example of combinatorial geometry specification. Areas 1 through 4 can be defined by whether or not they are inside or outside of the circle, triangle, or rectangle.	21
Figure 3: Cartesian direction cosines.	24
Figure 4: Example problem for determining the distance to a surface for a sphere located at the origin.	25
Figure 5: Sampling collision type.	28
Figure 6: Parallelization of response calculation through the master-slave paradigm.	41
Figure 7: Parallel scaling of response function generation.	43
Figure 8: Parallel efficiency of the response generation.	44
Figure 9: EPR assembly pin geometry for: (A) Fuel/Gadged Pin, (B) Guide Tube, (C) Guide Tube with Control Rod	49
Figure 10: EPR uncontrolled/controlled Assembly layout	50
Figure 11: EPR gaddged assembly layout.	52
Figure 12: HELIOS model of the uncontrolled 17x17 EPR assembly.	54
Figure 13: HELIOS model of the controlled 17x17 EPR assembly.	54
Figure 14: HELIOS model of the 17x17 gaddged EPR assembly.	55
Figure 15: Uncontrolled assembly pin fission density.	58
Figure 16: Controlled assembly pin fission density.	61
Figure 17: Gaddged assembly pin fission density.	64
Figure 18: Fission density for the uncontrolled assembly.	69
Figure 19: Fission density for the controlled assembly.	70
Figure 20: Fission density for the gaddged assembly.	71

SUMMARY

Stochastic Particle Response Calculator, SPaRC, is a new stochastic neutron transport code that has been developed and optimized for the computation of response functions for use in response matrix based whole-core transport solvers. SPaRC transports neutrons from a specified fixed source distribution and computes responses as neutrons stream through and then exit regions of interest. The code makes use of both multi-group and continuous energy nuclear data and takes advantage of parallel computing through the message passing interface (MPI). In order to test the neutron transport routine, various small benchmark problems were solved with SPaRC and compared to results generated with MCNP. Results show excellent agreement between the solutions generated by these codes for both multi-group and continuous energy calculations.

The responses generated by SPaRC have been tailored for use in the coarse mesh transport (COMET) method. COMET is a hybrid stochastic/deterministic method shown to compute fast and accurate solutions for a variety of nuclear systems. In order to obtain these solutions, COMET makes use of pre-computed response functions aggregated into a library for use in a deterministic iteration scheme. Previously these response functions were calculated with MCNP and took place before a transport calculation. SPaRC also generates these response functions for use with the COMET method, with the added capability of performing these calculations during the transport routine as needed. This on-the-fly capability for response generation enables the use of the COMET method for calculations where the state of a problem changes with time. SPaRC's ability to generate responses during a calculation eliminates the need for a fully pre-computed response library to cover the entire possible solution space, extending the capability of COMET to neutronics problems involving multi-physics feedback, such as thermal-hydraulic and depletion calculations.

Sample calculations on the reactor assembly level were performed in order to test the accuracy of the SPaRC generated response functions. First, responses were generated for uncontrolled, controlled, and gadded assemblies with both MCNP and SPaRC. Next, COMET calculations were performed using these two sets of responses for the different assembly types in order to generate eigenvalues and pin fission density distributions. The results generated from the MCNP and SPaRC responses agreed within 0.05% for the core eigenvalue and within 0.002% for pin powers.

SPaRC is a newly developed fixed-source radiation transport code. The neutron transport method has been benchmarked against the stochastic transport code MCNP with good agreement and new database management and creation routines have been developed to aid response generation. SPaRC introduces a response function flexibility to the COMET method that facilitates thermal hydraulic and depletion calculations.

CHAPTER 1

INTRODUCTION

For the design and safety of nuclear systems, it is important to have accurate models and simulations. In the case of nuclear power reactors, it is important to know the eigenvalue and the power distribution within the core at any moment in time. Traditional methods of generating solutions for these whole reactor core systems consist of a multi-stage approach. First, detailed transport calculations are performed on a lattice level such as a single fuel assembly. These calculations are typically two dimensional, use specular reflective boundary conditions to simulate the environment of the whole reactor, and make use of a pre-generated set of nuclear data tailored to the specific system. From these lattice level calculations, a library of spatially homogenized and energy collapsed cross sections is generated for each unique assembly type ^[1]. Then, using the library of homogenized nuclear data, solutions on the larger, whole core level are generated. This series of calculations introduces errors and the accuracy of the solution decreases as core heterogeneity increases. These errors are due to the homogenization of the cross sections as well as the approximation of the boundary conditions during the lattice calculation. In order to address these issues, the coarse mesh radiation transport (COMET) method was developed.

COMET is a hybrid deterministic stochastic method that has been shown to solve reactor problems fast and accurately. Much like the traditional methods of solving reactor problems, COMET uses a domain decomposition to divide the problem into unique coarse mesh regions. However, an angular flux expansion technique is used on the boundary instead of assuming a specular boundary condition. For each unique mesh region, rather than generating homogenized cross sections, both surface to surface and surface to volume response functions are stochastically generated. These responses are then incorporated into

a data library where they are used to deterministically generate fast and accurate results for large reactor systems. The COMET method has been proven to be a fast and accurate method to obtain whole-core solutions for multiple nuclear reactor designs including pressurized water reactors (PWRs)^[2], boiling water reactors (BWRs)^[3], Canada deuterium uranium reactors (CANDUs)^[4], and high-temperature gas-cooled reactors (HTGRs)^[5].

1.1 Motivation

The current implementation of COMET involves a multi-stage process. First, response functions are generated using the Monte Carlo n-particle transport code MCNP^[6]. Once the responses are generated, a routine is run to process the response data and then to create a database to store the responses. It is from this database that the responses are accessed during the deterministic calculations to generate solutions. If there is a need to update the database, similar steps need to be performed, but the post processing routine now appends to, instead of creates, the database.

Since updating the database and generating new responses is not a trivial procedure, it is important that the response database cover the entire solution space of a problem. However, this is not always possible in situations where the reactor state changes with time. Two such situations where the reactor state changes in time are in reactor depletion, where the material composition of the system changes with time, and in thermal-hydraulic calculations, where the temperature of the system changes with time. In these situations, the procedure of generating responses and then processing them into a database must be performed after each step since the future state of the problem is not known *a priori*. Thus, the previous COMET implementation of updating responses and managing the database does not easily facilitate these problems where the reactor state changes in time. In order for COMET to become a multi-physics code that can handle systems where the reactor state changes it is important that the response generation and database management routines be updated and improved upon.

1.2 Objectives

The objective of this dissertation is the development of an incident response generator that is optimized to generate on-the-fly response functions for COMET. This response generation ability, along with new response function database management routines, must allow COMET to perform depletion and thermal-hydraulic calculations. The response generation method must be flexible, allowing for arbitrary response specification, and must also be implemented in parallel since response generation is the most computationally expensive portion of a COMET calculation. The database management and creation routines must also be flexible, allowing for easy modification and access, to be able to facilitate future parallel deterministic calculations in COMET. All of these routines must also all be run in memory not only for ease of use, but also to save computational time.

1.3 Organization

This paper will first review the COMET methodology for solving nuclear systems. This will detail the domain decomposition, response generation, and the deterministic calculations all involved in solving a nuclear system with COMET. Next, a mathematical basis for stochastic neutron transport will be provided. Then the theoretical and practical details involved with transporting neutrons stochastically will be discussed. Having discussed stochastic transport in general, some specifics of the SPaRC response generation implementation will be detailed along with the new database management scheme. Next, having introduced the methodology of both COMET and SPaRC, benchmarks will be introduced that will test the codes. Various small fixed source benchmarks and their solutions will be compared to test the neutron transport routine of the SPaRC code with both multi-group and continuous energy cross sections. Finally, an EPR benchmark on the assembly level will be introduced for uncontrolled, controlled and gadded assembly types.

COMET solutions to these systems will then be compared for calculations using both the old MCNP and the new SPaRC generated responses.

CHAPTER 2

COMET METODOLOGY

For nuclear systems, it is important to know the angular flux distribution throughout the volumes or regions of interest. By obtaining the flux distribution, the eigenvalue of the system, the power distribution, and other reactions of interest can be obtained. The angular neutron flux in a system V with boundary ∂V can be solved for with the following Boltzmann transport equation,

$$\mathbf{H}\Psi(\bar{r}, \hat{\Omega}, E) = \frac{1}{k}\mathbf{F}\Psi(\bar{r}, \hat{\Omega}, E) \quad r \in V \quad (1)$$

with the following boundary condition,

$$\Psi(\bar{r}, \hat{\Omega}, E) = \mathbf{B}\Psi(\bar{r}', \hat{\Omega}', E') \quad \bar{r}, \bar{r}' \in \partial V \quad \hat{n} \cdot \hat{\Omega} < 0 \text{ and } \hat{n} \cdot \hat{\Omega}' > 0 \quad (2)$$

This is a steady state equation with $\Psi(\bar{r}, \hat{\Omega}, E)$ representing the angular neutron flux at position \bar{r} with direction $\hat{\Omega}$, and energy E . The system is defined in a volume V with boundary ∂V . The value k represents the global eigenvalue, a value to scale the fission source of neutrons in order to ensure a balance in Equation 1, and \hat{n} represents the outward normal on the boundary. \mathbf{B} represents the general boundary condition operator and \mathbf{H} and \mathbf{F} are operators defined as follows,

$$\mathbf{H} = \hat{\Omega} \cdot \nabla + \sigma_t(\bar{r}, E) - \int dE' \int_{4\pi} d\hat{\Omega}' \sigma_s(\bar{r}; \hat{\Omega}', E' \rightarrow \hat{\Omega}, E) \quad (3)$$

$$\mathbf{F} = \frac{\chi(\bar{r}, E)}{4\pi} \int dE' \int_{4\pi} d\hat{\Omega}' \nu(E') \sigma_f(\bar{r}, E') \quad (4)$$

where $\sigma_t(\bar{r}, E)$ is the total cross section, $\sigma_s(\bar{r}; \hat{\Omega}', E' \rightarrow \hat{\Omega}, E)$ is the scattering cross section for neutrons scattering from direction and energy $\hat{\Omega}', E'$ to $\hat{\Omega}, E$, $\chi(\bar{r}, E)$ is the energy distribution function of fission neutrons, $\nu(E')$ is the number of neutrons produced from fission, and $\sigma_f(\bar{r}, E')$ is the fission cross section.

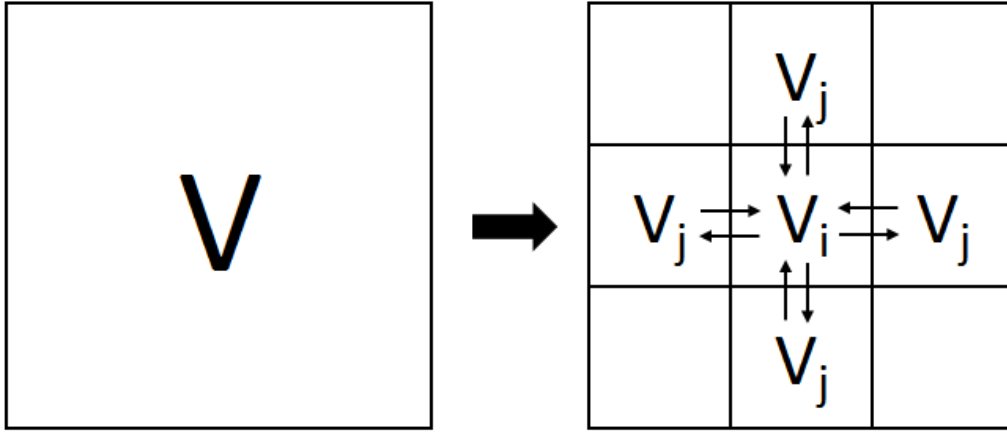


Figure 1. Spatial domain decomposition, the volume V is split into non-overlapping regions V_{ij} with boundary conditions dependent on adjacent volumes.

The first step in the COMET methodology is to split the spatial domain of the problem into non-overlapping coarse meshes (see Figure 1). This spatial decomposition transforms the larger transport problem into the smaller local problems given below,

$$\mathbf{H}\Psi_i(\bar{r}, \hat{\Omega}, E) = \frac{1}{k} \mathbf{F}\Psi_i(\bar{r}, \hat{\Omega}, E) \quad r \in V_i \quad (5)$$

with the following boundary condition,

$$\Psi_i(\bar{r}, \hat{\Omega}, E) = \Psi_{is}(\bar{r}, \hat{\Omega}, E) \quad \bar{r} \in \partial V_{is} \quad \hat{n}_{is}^+ \cdot \hat{\Omega} < 0 \quad (6)$$

where ∂V_{is} represents the surface of mesh i with volume V_i , \hat{n}_{is}^+ represents the outward normal on ∂V_{is} , and $\Psi_{is}(\bar{r}, \hat{\Omega}, E)$ is the incoming angular flux from adjacent coarse meshes. It should be noted that the eigenvalue k in Equation 5 is the global eigenvalue of the entire problem and not just the eigenvalue of that specific coarse mesh.

The spatial decomposition in principle does not introduce any approximations to the system. If the incoming angular fluxes on the boundary $\Psi_{is}(\bar{r}, \hat{\Omega}, E)$ are known beforehand, the angular flux throughout the coarse mesh $\Psi_i(\bar{r}, \hat{\Omega}, E)$ can be obtained. However, since these boundary fluxes are not known beforehand, the inward and outward angular fluxes on the boundaries are represented in terms of orthogonal expansion functions,

$$\Psi_{is}^\pm(\bar{r}, \hat{\Omega}, E) = \sum_{s,m} J_{is}^{\pm,m} \Gamma_m(\bar{r}, \hat{\Omega}, E) \quad \bar{r} \in \partial V_{is} \quad \hat{n}_{is}^\pm \cdot \hat{\Omega} > 0 \quad (7)$$

where $\Gamma_m(\bar{r}, \hat{\Omega}, E)$ are orthogonal expansion functions and $J_{is}^{\pm,m}$ are the associated expansion coefficients. Using this angular flux representation and using the fact that the Boltzmann transport equation is linear, the solution to the angular flux within a mesh can be constructed as,

$$\Psi_i(\bar{r}, \hat{\Omega}, E) = \sum_{s,m} J_{is}^{-,m} R_{is}^m(\bar{r}, \hat{\Omega}, E) \quad \bar{r} \in \partial V_i \quad (8)$$

where $R_{is}^m(\bar{r}, \hat{\Omega}, E)$ is the solution to the fixed source problem,

$$HR_{is}^m(\bar{r}, \hat{\Omega}, E; k) = \frac{1}{k} FR_{is}^m(\bar{r}, \hat{\Omega}, E; k) \quad r \in V_i \quad (9)$$

with the following boundary condition,

$$R_{is}^m(\bar{r}, \hat{\Omega}, E; k) = \Gamma_m(\bar{r}, \hat{\Omega}, E) \quad \bar{r} \in \partial V_{is} \quad \hat{n}_{is}^+ \cdot \hat{\Omega} < 0 \quad (10)$$

It can be seen that $R_{is}^m(\bar{r}, \hat{\Omega}, E; k)$ corresponds to the angular flux distribution within a mesh due to an incoming flux corresponding to the distribution $\Gamma_m(\bar{r}, \hat{\Omega}, E)$ imposed on the mesh surface.

For the choice of expansion functions, it is natural that the 0th order expansion function represent the isotropic flux. Since the neutron distribution in a reactor core is isotropic on average it is important that the magnitude of the partial current is preserved. To meet these requirements, the following orthogonality condition is enforced,

$$\int dE \int_{\partial V_{is}} d\bar{r} \int_{\hat{n}_{is}^+ \cdot \hat{\Omega} > 0} d\hat{\Omega} (\hat{n}_{is}^+ \cdot \hat{\Omega}) \Gamma_m(\bar{r}, \hat{\Omega}, E) \Gamma_{m'}(\bar{r}, \hat{\Omega}, E) = A_m \delta_{mm'} \quad (11)$$

where A_m is a constant and $\delta_{mm'}$ is the Kronecker delta. Previous work into the choice of expansion functions has been completed. It was found that expansion functions constructed as a product of Legendre polynomials $P_n(x)$ and Chebyshev polynomials of the second kind $U_n(x)$ give good results to a number of nuclear systems. The angular flux on the surface is represented using the following expansion,

$$\Gamma_{ijk}(\bar{r}, \hat{\Omega}, E) = P_i(\bar{r}) U_j(\cos \theta) P_k(\cos \varphi) \delta(E - E_g) \quad (12)$$

with the position variables and the cosine of φ represented with Legendre polynomials and the cosine of θ being represented by Chebyshev polynomials of the second kind. The energy variable is treated with the Dirac delta function signifying a multi-group formulation. The formulations for obtaining the Chebyshev polynomials expansions can be obtained using Equations 13 and the Legendre expansions can similarly be obtained using Equation 14. From these equations, the 0th order expansion can be seen to represent an isotropic flux.

$$\begin{aligned}
 U_0(\mu) &= 1 \\
 U_1(\mu) &= 2\mu \\
 U_{n+1}(\mu) &= 2\mu U_n(\mu) - U_{n-1}(\mu), \quad n \geq 1
 \end{aligned} \tag{13}$$

$$\begin{aligned}
 P_0(x) &= 1 \\
 P_1(x) &= x \\
 (n+1)P_{n+1}(x) &= (2n+1)xP_n(x) - nP_{n-1}(x), \quad n \geq 1
 \end{aligned} \tag{14}$$

2.1 Response Generation

The outgoing and incoming partial currents (expansion coefficients) for a surface s' and a coarse mesh i are related by the following equation,

$$J_{is'}^{+,m'} = \sum_{s,m} R_{iss'}^{mm'} J_{is}^{-,m} \tag{15}$$

where $R_{iss'}^{mm'}$ is the surface-to-surface response function related to $R_{is}^m(\bar{r}, \hat{\Omega}, E; k)$ by the following relation,

$$R_{iss'}^{mm'}(k) = \int dE \int_{\partial V_{is'}} d\bar{r} \int_{\hat{n}_{is'}^+ \cdot \hat{\Omega} > 0} d\hat{\Omega} (\hat{n}_{is'}^+ \cdot \hat{\Omega}) \Gamma_{m'}(\bar{r}, \hat{\Omega}, E) R_{is}^m(\bar{r}, \hat{\Omega}, E; k) \quad (16)$$

Here $R_{iss'}^{mm'}$ can be seen to be the magnitude of the outgoing flux from surface s' in moment m' from a unit incoming flux distributed on surface s .

For each unique coarse mesh i both surface-to-surface $R_{iss'}^{mm'}(k)$ and surface-to-volume $R_{is}^m(\bar{r}, \hat{\Omega}, E; k)$ response functions have to be calculated. This response function generation is done with stochastic neutron transport in order to make use of its ability to model complex geometry and easily treat continuous expansion functions. The choice of a stochastic code also allows for the direct treatment of the energy variable instead of just a multi-group formulation. During the stochastic response calculations, particles are first spawned from an incoming distribution $\Gamma_m(\bar{r}, \hat{\Omega}, E)$. The particles are then tracked through the coarse mesh and volume responses of interest are calculated by path length tallies as described in Chapter 3. When a particle leaves the coarse mesh through a surface, the surface-to-surface response function can then be calculated through the following equation,

$$R_{iss'}^{mm'} = \frac{1}{N} \sum_{n, \bar{r} \in \partial V_s} \Gamma_{m'}(\bar{r}_n, \hat{\Omega}_n, E_n) w_n \quad (17)$$

where N is the total number of source particles, $\bar{r}_n, \hat{\Omega}_n, E_n$ and w_n are the position, angle, energy, and weight of particle n as it escapes through coarse mesh surface ∂V .

With stochastic calculations there is an inherent uncertainty associated with the solutions. The sample variance for the responses is calculated using the following equation,

$$\delta^2 [R_{iss'}^{mm'}] = \frac{1}{N} \sum [\Gamma_{m'}(\bar{r}_n, \hat{\Omega}_n, E_n) w_n]^2 - \left[\frac{1}{N} \sum \Gamma_{m'}(\bar{r}_n, \hat{\Omega}_n, E_n) w_n \right]^2 \quad (18)$$

It was seen earlier that the response functions are dependent on the global eigenvalue k . Since the eigenvalue is not known beforehand, responses are calculated at multiple bounding eigenvalues and then can be interpolated upon for a given eigenvalue using the following equation,

$$R_{iss'}^{mm'}(k) = \frac{1/k - 1/k_1}{1/k_2 - 1/k_1} R_{iss'}^{mm'}(k_1) + \frac{1/k_2 - 1/k}{1/k_2 - 1/k_1} R_{iss'}^{mm'}(k_2) \quad (19)$$

where the global eigenvalue k lies between response libraries generated at k_1 and k_2 . As long as the response library generated encompasses the global eigenvalue the responses can be interpolated in order to obtain the solution. Other methods have been developed to get around this need for generating responses at multiple k values including a perturbation calculation method^[7] and a fission collision separation method^[8]. The SPaRC responses generated for this paper use the k grid scheme.

Responses only have to be generated for unique coarse meshes based on their geometry and material composition. Thus for systems such as nuclear reactor cores where there are repeated assemblies as well as repeated pins, significant improvements in computational efficiency can be made.

2.2 Deterministic Iteration Scheme

Once the responses have been generated stochastically, they are processed and then formatted into a database. Then an iterative deterministic method is used to generate solutions for the system by iterating upon the responses from the coarse meshes that make up the system. The deterministic solution involves both outer iterations on the eigenvalue k and inner iterations on the currents between meshes. The COMET deterministic solution method is as follows:

- (A) First an initial guess is made for both the global eigenvalue k and the expansion coefficients J .
- (B) The responses are updated for the eigenvalue k using Equation 19.
- (C) Inner iterations are performed to solve for the currents using the following equation,

$$\sum_{s,m} R_{iss'}^{mm'}(k) J_{is}^{-,m} = \lambda J_{is'}^{+,m'} \quad (20)$$

- (D) Once the currents are converged, the global eigenvalue is then updated using the following equation,

$$\begin{aligned} k(u+1) &= \frac{\text{Production}(u)}{\text{Absorption}(u) + \text{Leakage}(u)} \\ &= \frac{\sum_{i,s,m} J_{is}^{-,m'}(u) \int dE \int_{V_i} d\bar{r} \int_{4\pi} d\hat{\Omega} v \sigma_f R_{is}^m(\bar{r}, \hat{\Omega}, E; k(u))}{\sum_{i,s,m} J(u) \int dE \int_{V_i} d\bar{r} \int_{4\pi} d\hat{\Omega} \sigma_a R_{is}^m(\bar{r}, \hat{\Omega}, E; k(u)) + \sum_{\partial V_{is} \subset \partial V} (J_{is}^{+,0}(u) - J_{is}^{-,0}(u))} \end{aligned} \quad (21)$$

where u is the outer iteration index. This equation is a formulation of the neutron balance equation accounting for neutron production from fission and neutron losses from absorption and leakage.

- (E) The steps (B)-(D) are repeated until the following convergence criterion is satisfied,

$$\left| \frac{k(u+1)}{k(u)} \right| < \epsilon_k \quad (22)$$

Once the system has converged for both the eigenvalue and interface coefficients, the values of interest within a coarse mesh can be calculated using the surface to volume responses and the incoming interface currents.

Many improvements have been made to speed up the deterministic calculations. Both a low order acceleration routine and a Chebyshev acceleration method have been used in order to speed up convergence to the global eigenvalue. A more detailed discussion of these acceleration routines as well as a detailed overview of the COMET method can be found in Reference 9.

CHAPTER 3

STOCHASTIC TRANSPORT METHODOLOGY

Neutron transport through a medium can be understood as a stochastic process. As a neutron traverses through a material, the total cross section defines the probability that a neutron will have a collision over a certain path length. Then, if the neutron has a collision, the probability of a certain type of collision is based on the individual cross sections of the different collision types. Since the neutron cross sections define probabilities of interaction rather than certainties, random numbers can be used to sample the events a neutron experiences while traveling through a system. Stochastic neutron transport is synonymous to running a physical experiment where the neutron is tracked step by step as it travels and interacts with a medium. By simulating many neutrons, the neutron flux of the problem can be determined as the flux is the mean value of the neutron distribution function. By simulating a larger number of neutrons, the mean behavior of all the neutrons in the system is obtained with greater accuracy. The rest of this chapter provides a mathematical basis for stochastic neutron transport, describes the details involved in transporting a neutron through a material, and goes over some practical implementation details.

3.1 Mathematical Foundation for Stochastic Neutron Transport

The purpose of a stochastic neutron transport code is to solve for the Boltzmann transport equation which can be formulated as,

$$\begin{aligned}
& \frac{1}{v} \frac{\partial \psi}{\partial t}(\bar{r}, \hat{\Omega}, E, t) + \hat{\Omega} \cdot \nabla \psi(\bar{r}, \hat{\Omega}, E, t) + \sigma_t(\bar{r}, E) \psi(\bar{r}, \hat{\Omega}, E, t) \\
& = \int dE' \int_{4\pi} d\hat{\Omega}' \sigma_s(\bar{r}; \hat{\Omega}', E' \rightarrow \hat{\Omega}, E) \psi(\bar{r}, \hat{\Omega}', E', t) \\
& + \frac{\chi(\bar{r}, E)}{4\pi} \int dE' \int_{4\pi} d\hat{\Omega}' \nu(E') \sigma_f(\bar{r}, E') \psi(\bar{r}, \hat{\Omega}', E', t) + S(\bar{r}, \hat{\Omega}, E, t)
\end{aligned} \tag{23}$$

where $\psi(\bar{r}, \hat{\Omega}, E, t)$ is the angular flux at position \bar{r} with direction $\hat{\Omega}$ and energy E at time t , v is the velocity of the neutron, $S(\bar{r}, \hat{\Omega}, E, t)$ is an external source not dependent on the neutron flux and the other variables are as defined in Chapter 2. The equation can be modified by using the method of characteristics to obtain the flux at position \bar{r} along direction $\hat{\Omega}$ at time t . To do this a path length variable s is introduced that goes through position and angle. It can be seen that,

$$\frac{d\psi}{ds} = \frac{\partial \psi}{\partial t} \frac{dt}{ds} + \frac{\partial \psi}{\partial x} \frac{dx}{ds} + \frac{\partial \psi}{\partial y} \frac{dy}{ds} + \frac{\partial \psi}{\partial z} \frac{dz}{ds} \tag{24}$$

and for Cartesian coordinates,

$$\frac{1}{v} \frac{\partial \psi}{\partial t} + \hat{\Omega} \cdot \nabla \psi = \frac{1}{v} \frac{\partial \psi}{\partial t} + \Omega_x \frac{\partial \psi}{\partial x} + \Omega_y \frac{\partial \psi}{\partial y} + \Omega_z \frac{\partial \psi}{\partial z} \tag{25}$$

By equating both Equation 24 and 25 the following expression can be obtained,

$$\frac{d\psi}{ds} = \frac{1}{v} \frac{\partial \psi}{\partial t} + \hat{\Omega} \cdot \nabla \psi \tag{26}$$

Then by equating orthogonal terms the following relations can be obtained,

$$\begin{aligned}
\frac{1}{v} \frac{\partial \psi}{\partial t} &= \frac{\partial \psi}{\partial t} \frac{dt}{ds} \rightarrow \frac{dt}{ds} = \frac{1}{v} \rightarrow t = t_0 + \frac{s}{v} \\
\Omega_x \frac{\partial \psi}{\partial x} &= \frac{\partial \psi}{\partial x} \frac{dx}{ds} \rightarrow \frac{dx}{ds} = \Omega_x \rightarrow x = x_0 + s\Omega_x \\
\Omega_y \frac{\partial \psi}{\partial y} &= \frac{\partial \psi}{\partial y} \frac{dy}{ds} \rightarrow \frac{dy}{ds} = \Omega_y \rightarrow y = y_0 + s\Omega_y \\
\Omega_z \frac{\partial \psi}{\partial z} &= \frac{\partial \psi}{\partial z} \frac{dz}{ds} \rightarrow \frac{dz}{ds} = \Omega_z \rightarrow z = z_0 + s\Omega_z
\end{aligned} \tag{27}$$

where t_0 , x_0 , y_0 , and z_0 are constants and the position variables can be combined to obtain,

$$\bar{r} = \bar{r}_0 + s\hat{\Omega} \tag{28}$$

Equation 23 can then be rewritten using these relations to obtain the following transport equation,

$$\begin{aligned}
&\frac{d}{ds} \psi \left(\bar{r}_0 + s\hat{\Omega}, \hat{\Omega}, E, t_0 + \frac{s}{v} \right) + \sigma_t(\bar{r}_0 + s\hat{\Omega}, E) \psi \left(\bar{r}_0 + s\hat{\Omega}, \hat{\Omega}, E, t_0 + \frac{s}{v} \right) \\
&= \int dE' \int_{4\pi} d\hat{\Omega}' \sigma_s(\bar{r}_0 + s\hat{\Omega}; \hat{\Omega}', E' \rightarrow \hat{\Omega}, E) \psi \left(\bar{r}_0 + s\hat{\Omega}, \hat{\Omega}', E', t_0 + \frac{s}{v} \right) \\
&+ \frac{\chi(\bar{r}_0 + s\hat{\Omega}, E)}{4\pi} \int dE' \int_{4\pi} d\hat{\Omega}' \nu(E') \sigma_f(\bar{r}, E') \psi \left(\bar{r}_0 + s\hat{\Omega}, \hat{\Omega}', E', t_0 + \frac{s}{v} \right) \\
&\quad + S \left(\bar{r}_0 + s\hat{\Omega}, \hat{\Omega}, E, t_0 + \frac{s}{v} \right)
\end{aligned} \tag{29}$$

By using an integrating factor and integrating over the phase space the following relation can be obtained for the angular flux,

$$\begin{aligned} \psi(\bar{r}, \widehat{\Omega}, E, t) = & \int_0^\infty e^{-\tau} \left(\int dE' \int_{4\pi} d\widehat{\Omega}' \sigma_s(\bar{r}_0 - s\widehat{\Omega}; \widehat{\Omega}', E' \rightarrow \widehat{\Omega}, E) \psi\left(\bar{r}_0 - \right. \right. \\ & \left. \left. s\widehat{\Omega}, \widehat{\Omega}', E', t_0 - \frac{s}{v}\right) \right) ds + \int_0^\infty e^{-\tau} \frac{\chi(\bar{r}_0 + s\widehat{\Omega}, E)}{4\pi} \int dE' \int_{4\pi} d\widehat{\Omega}' \nu(E') \sigma_f(\bar{r}, E') \psi\left(\bar{r}_0 - \right. \\ & \left. s\widehat{\Omega}, \widehat{\Omega}', E', t_0 - \frac{s}{v}\right) ds + \int_0^\infty e^{-\tau} S\left(\bar{r}_0 + s\widehat{\Omega}, \widehat{\Omega}, E, t_0 - \frac{s}{v}\right) ds \end{aligned} \quad (30)$$

where τ is the optical distance and is defined as,

$$\tau = \int_0^\infty \sigma_t(\bar{r} - s\widehat{\Omega}, E) ds' \quad (31)$$

In operator notation Equation 30 can then be represented as

$$\psi = \mathbf{K}\psi + S' \quad (32)$$

where \mathbf{K} is the integral operator and S' is the attenuated source. A solution to Equation 32 can then be written in terms of how many collisions a neutron has undergone before reaching a location. This formulation is as follows,

$$\begin{aligned} \psi_0 &= S' \\ \psi_1 &= \mathbf{K}\psi_0 \\ &\vdots \\ \psi_{n+1} &= \mathbf{K}\psi_n \end{aligned} \quad (33)$$

which can then be written in the following summation form if the series converges,

$$\psi = \sum_{n=0}^{\infty} \psi_n \quad (34)$$

Equation 34 is known as a von Neumann series. It can be seen from Equation 33 that ψ_n represents the angular flux at a point that has made n collisions. Thus ψ_0 is the angular flux at a point due to neutrons having no collisions traveling from the source, ψ_1 is the angular flux at a point from neutrons undergoing one collision, and so on. The stochastic tracking of neutrons that have not undergone a collision gives an estimate for ψ_0 , and then the continued tracking of particles that have undergone collisions gives estimates for ψ_1 , ψ_2 , etc. The stochastic process thus estimates the von Neumann series solution for the integral formation of the transport equation. For a detailed description of this mathematical derivation readers are referred to Reference 10.

3.2 Transport Implementation

A mathematical basis has been provided for the solution to the Boltzmann transport equation. Next, the practical implementation details of transporting neutrons through a medium and obtaining results will be discussed. For stochastic neutron transport, individual neutrons and their interactions are tracked as neutrons travel from a given source and then leave the system of interest. By simulating a large number of neutrons and recording their mean behavior, solutions of interest are obtained. The process of running a stochastic neutron transport simulation is as follows:

- 1) First, the problem must be defined. This includes specifying the following:
 - a. The geometry of system. This is done by defining surfaces and then defining regions bounded by those surfaces.
 - b. The material compositions that fill the regions of the problem, including both the isotopic makeup, density, and temperature.
 - c. The calculation type, whether continuous energy or multi-group, and the location of the data libraries used for the calculation.

- d. The specification for the source, which includes the neutron location, direction, and energy.
 - e. The boundary conditions of the system.
 - f. The results of interest to be recorded.
 - g. The run parameters of the calculation including the number of particles to simulate, parallel computing parameters, etc.
- 2) Once the problem is sufficiently defined, a neutron history is started by sampling from the specified source distribution. In this step, the neutron is assigned a position, direction of travel, energy, and weight. Then, based on the position of the particle, the region containing the particle is defined.
 - 3) Next, the distance that the neutron will travel until it has a collision is sampled in terms of mean free path.
 - 4) Based on the current region/material the neutron is in, the total cross section as well as other cross sections of interest are obtained from the data library.
 - 5) Using the position of the particle and its direction as well as the geometry specification, the distances to the boundaries of the problem regions along the path of the neutron are determined.
 - 6) Depending upon how far the boundary is and how far the distance to the next collision, the neutron either makes a collision along its current path or reaches the boundary and goes to another region. The neutron position is then updated to be at the collision site or at the boundary.
 - 7) If a collision happens, the type of collision is sampled based upon the cross sections for each reaction type. Depending on the type of collision, a new neutron is spawned with a different energy and direction based off the nuclear data. If more than one neutron is produced from the collision, extra neutrons are stored in a bank until the tracking of the current neutron is terminated. The

neutron coming out of a collision then acts as the source neutron in step 2) and the process is repeated starting at step 3).

- 8) If no collision happens before the neutron reaches the boundary, the neutron is transported along the path to just on the other side of the boundary. The distance to collision is then updated by subtracting the distance that the neutron has travelled. The transport history then starts over at step 4).
- 9) If the particle crosses a boundary out of the system of interest, the history is then terminated. The properties of the exiting neutrons are then used to generate the surface to surface response functions.
- 10) During the calculation, when neutrons enter regions of interest such as fuel pins, tallies are made to record quantities of interest.

The previous list provides an overview of the steps involved during a stochastic neutron transport simulation. Next, more details will be provided into how the transport routine is implemented in SPaRC and other stochastic transport codes.

3.2.1 Pseudo Random Number Generation

For stochastic calculations, values of interest for neutron transport are often given in distributions or probabilities. In order to sample correctly from these distributions without biases, it is important to have good random numbers. It is important that the numbers are random, a requirement ensured by having a uniform distribution, and have a long period so that numbers do not repeat during the calculation. For practical purposes, the random numbers should be reproducible so as to be able to perform perturbation calculations as well as to allow the ability to reproduce results. The generation method should also be fast and efficient since multiple random numbers are required to perform the transport of just one neutron. In order to fill the previous requirements, many algorithms have been developed to generate pseudo random numbers over an interval. There has been

a great amount of research in developing these random number algorithms as well as in developing tests in order to check their randomness. However, choosing a suitable pseudo random number generator (PRNG) for a particular problem is not always easy^[11]. SPARC makes use of the Mersenne Twister^[12] PRNG to generate random numbers. This is a PRNG with a long period of $2^{19937} - 1$, has a relatively low number generation time, and passes many of the common tests for randomness.

3.2.2 Geometry Specification

The first step for any stochastic calculation is to define the problem. SPARC makes use of combinatorial geometry in order to specify the geometry and regions of the problem. In this method, bodies such as spheres, parallelepipeds, and cylinders are used to build the problem geometry. Then different regions can be defined by indicating whether the region is inside or outside of a given body. Figure 2 shows a simple 2D example of this.

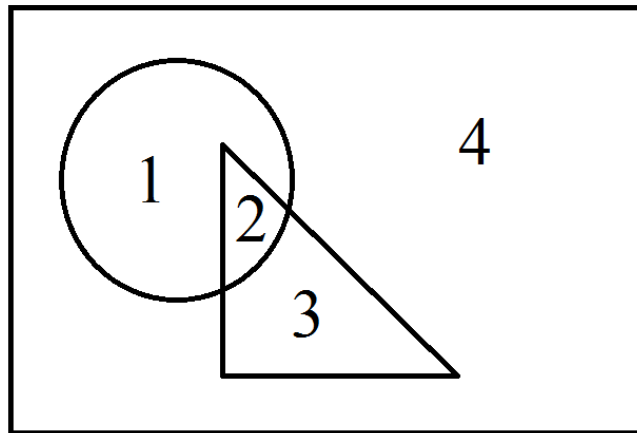


Figure 2. An example of combinatorial geometry specification. Areas 1 through 4 can be defined by whether or not they are inside or outside of the circle, triangle, or rectangle.

In the 2D geometry represented in Figure 2 areas 1 through 4 can be specified by indicating whether they fall inside or outside a given shape as well as using AND and OR logical constructions. With these specifications, regions can be specified with relation to

the given surfaces. Table 1 gives an example of how some regions might be specified. By knowing the position of the particle as well as the mathematical formulas that describe the surfaces of the geometry, it is possible to determine whether the particle is within a region or not and then determine which region it is currently located in. A simple example of this would be to determine if a particle located at position x, y, z is located within a sphere of radius R located at the origin. In this case, if $\sqrt{x^2 + y^2 + z^2} < R$ then the particle is currently located within the sphere; otherwise particle is located outside of the sphere.

Table 1. Combinatorial geometry specifications for regions in Figure 2.

Region	Specification
1	inside sphere AND outside triangle
2	inside sphere AND inside triangle
3	outside sphere AND inside triangle
4	inside rectangle AND outside sphere AND outside triangle
1+2+3	inside sphere OR inside triangle

3.2.3 Sampling the Distance to a Collision

Once a neutron has been created from a source distribution and given a position, direction, and energy, the distance the particle will travel before it has a collision must be sampled. For a neutron traveling along a path the probability that a collision will happen is characterized by the total cross section σ_t . Over a distance s the probability of collision within a distance ds is $\sigma_t ds$, and the probability that a neutron does not have a collision over a distance s is $e^{-\sigma_t s}$. The combination of these probabilities is as follows,

$$p(s) = \sigma_t e^{-\sigma_t s} ds \quad (35)$$

In order to sample the distance traveled before a collision, the following can be solved,

$$RN = \int_0^l \sigma_t e^{-\sigma_t s} ds \quad (36)$$

where RN , is a random number on the interval $[0,1)$ and l is the distance to collision. Solving for the distance to collision the following relation is obtained,

$$l = \frac{-\ln(RN)}{\sigma_t} \quad (37)$$

where $RN - 1$ was set to RN since it represents the same distribution of random numbers.

It can be seen from Equation 37 that the distance traveled to the next collision is dependent upon the total cross section within the current region. If a particle travels through multiple regions before a collision happens, Equation 37 must be used to obtain a new distance to collision upon entering a new region. In order to avoid this, Equation 37 can be reformulated in terms of mean free path. Noting that the mean free path of a neutron is $\lambda = 1/\sigma_t$, Equation 37 becomes,

$$d = -\ln(RN) \quad (38)$$

where d is the distance to collision in mean free paths. For the SPaRC code, upon the generation of a new neutron, Equation 38 is used to sample the distance to collision.

3.2.4 Determining Distances to Surfaces

The surfaces that define a geometry have a mathematical equation that can be used to determine how far a particle has to travel in order to intersect them. Table 2 specifies the equations for some simple geometries used to set up the geometry of a transport simulation.

Table 2. Formulas for some simple geometries.

Surface	Specifying Equation
Plane	$ax + by + cz = -d$
Sphere	$(x - a)^2 + (y - b)^2 + (z - c)^2 = R^2$
Cylinder	$(x - a)^2 + (y - b)^2 = R^2$

SPaRC uses a Cartesian coordinate system in order to track neutrons. The position of a particle is defined by x , y , and z and the direction cosines along those directions are given by the following relation,

$$\begin{aligned} u &= \sin \theta \cos \varphi \\ v &= \sin \theta \sin \varphi \\ w &= \cos \theta \end{aligned} \quad (39)$$

where θ is the polar angle from the z -axis and φ is the polar angle from the x -axis on the xy -plane. A pictorial representation of the directional cosines of the Cartesian coordinate system can be seen in Figure 3.

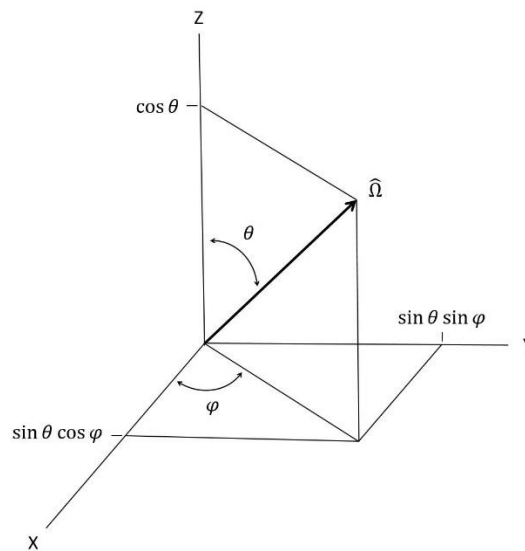


Figure 3. Cartesian direction cosines.

In order to see how the distance to surfaces is calculated, a simple 2D example problem will be introduced. Figure 4 represents a situation where a neutron characterized by position (x_o, y_o) and direction $\widehat{\Omega}$ travels and intersects with a circle located at the origin.

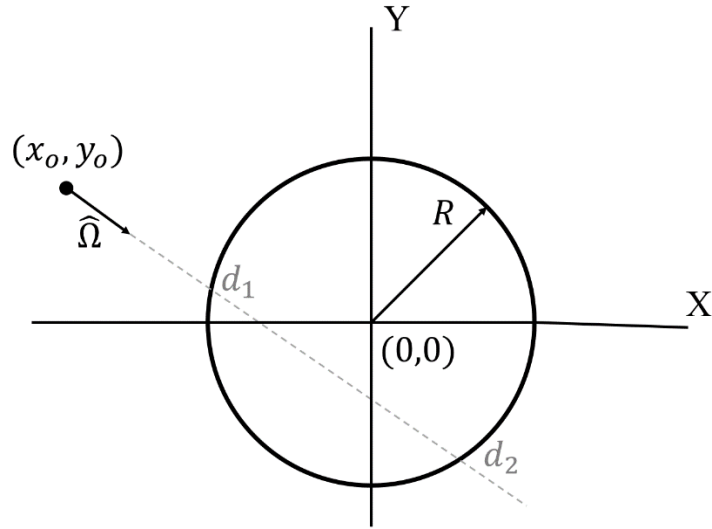


Figure 4. Example problem for determining the distance to a surface for a sphere located at the origin.

At any point in time, a neutron being tracked can be characterized by its position and direction. In order to see if a neutron will intersect a surface, a path length variable s can be introduced along the direction of travel of the neutron. If a particle located at a position (x_o, y_o) travels a distance s along direction $\widehat{\Omega}$, the new position can be calculated using the following equation,

$$\begin{aligned} x &= x_o + us \\ y &= y_o + vs \end{aligned} \tag{40}$$

where u and v , are the direction cosines in two dimensions. Next, the equation for a circle located at the origin can be defined as,

$$x^2 + y^2 = R^2 \quad (41)$$

where R is the radius of the sphere. By plugging in the relations from Equation 40 into Equation 41 and then simplifying, the following expression can be obtained,

$$s^2 + 2s\bar{r} \cdot \hat{\Omega} + x_o^2 + y_o^2 - R^2 = 0 \quad (42)$$

where,

$$\bar{r} \cdot \hat{\Omega} = ux_o + vy_o \quad (43)$$

Solving for Equation 42 gives the following solutions,

$$s = -\bar{r} \cdot \hat{\Omega} \pm \sqrt{(\bar{r} \cdot \hat{\Omega})^2 - (x_o^2 + y_o^2 - R^2)} \quad (44)$$

Using this equation one can determine the position of a particle. If the solutions are positive, they correspond to the distances of entry and exit into a surface (d_1 and d_2 in Figure 4). If both solutions are negative, the surface lies in the opposite direction of the neutron path and thus the neutron will not intersect the surface. If one solution is positive and one solution negative, the particle is located within the surface with the positive value corresponding to the distance to exit the surface. Finally, If the discriminant is negative, the surface is not in the path of the particle and thus the particle will not enter the surface because there are no solutions to Equation 44.

The procedure to determine distances to surfaces can be done for all of the surfaces that define a problem. By determining the distances to the surfaces as well as knowing the geometry specification as defined in Section 3.2.2, the region that a neutron is in as well as the distance until the neutron exits that region can be calculated.

3.2.5 Determining Whether a Collision Happens Within a Region

In Section 3.2.3 the distance a neutron will travel in mean free paths before a collision was determined and in Section 3.2.4 the procedure for calculating the distances to surfaces (and therefore region boundaries) was described. With these values, as well as the total neutron cross section of the current problem region, whether a neutron has a collision or whether it reaches the boundary can be determined. First, the distance to the boundary can be converted to be in terms of mean free path using the total cross section of that region and remembering that $\lambda = 1/\sigma_t$. Then, if the distance to the boundary in mean free paths is greater than the distance to sampled distance to collision, a collision happens within the current region and the neutron is transported the distance determined by the sampled distance to collision. If the distance to the boundary is less than the distance to collision, the neutron is transported to the boundary and the distance to collision is updated by subtracting the distance to the boundary. If the neutron reaches the boundary, the process is repeated until the neutron either leaves the system or a collision is sampled.

3.2.6 Sampling Collision Type

Once it has been determined that a neutron has had a collision, the type of collision can then be determined by sampling from all the possible reaction types. The probability that a certain reaction happens is just the cross section for that reaction divided by the total cross section. Figure 5 shows a case where three different reactions are possible namely scattering, absorption, and fission. Noting that the total cross section for this case can be represented as a sum of the three reactions, namely $\sigma_t = \sigma_s + \sigma_a + \sigma_f$, the sum of the separate reactions divided by the total sum to one. Given a random number, RN, distributed over an interval (0, 1) the type of reaction can be determined by where the number falls on the line (Table 3).

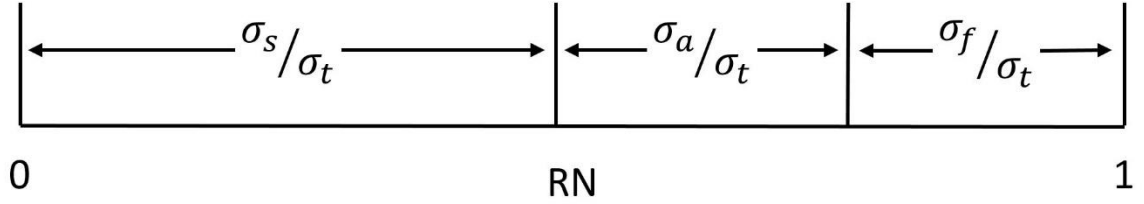


Figure 5. Sampling collision type.

Table 3. Sampling collision type.

Condition	Collision Type
$RN < \sigma_s/\sigma_t$	Scattering
$\sigma_s/\sigma_t < RN < \sigma_s/\sigma_t + \sigma_a/\sigma_t$	Absorption
$\sigma_s/\sigma_t + \sigma_a/\sigma_t < RN$	Fission

The nuclear data used to determine when a collision happens, the type of collision, and the result of the collision come in two formulations. There is a multi-group formulation, where the energy variable is integrated into a group structure, and a continuous energy formulation where the neutron can take any energy value. These two energy representations and some practical details involved in neutron transport will be discussed next.

3.2.7 Multi-group energy formulation

Multi-group treatment involves reducing the energy spectrum down to a finite number of discrete energy groups by integration over the energy variable. In order to create nuclear data for these energy groups, the continuous energy data must be transformed. This transformation involves integration of the data over the range of an energy group. Continuous energy cross sections are condensed down in energy using Equation 45.

$$\sigma_g = \frac{\int_{E_g}^{E_{g-1}} dE \sigma(E) \phi_{approx}(\bar{r}, E)}{\int_{E_g}^{E_{g-1}} dE \phi_{approx}(\bar{r}, E)} \quad (45)$$

where E_g are the energy group bounds and ϕ_{approx} is an assumed scalar flux. It is important that during this process of creating multi-group data that the reaction rate ($\int \varphi \sigma dE$) be conserved. This conservation requires that the scalar flux φ for the system is known beforehand. Since the flux is not known beforehand it must be approximated. This is often done by running a smaller calculation that aims to represent the system as a whole. This approximation often leads to errors in the solution if not done correctly, and is one of the drawbacks of the multi-group formulation.

Table 4. Multi-group cross section definitions.

Cross Section	Definition
σ_t^g	Total cross section for group g , probability of a neutron having any interaction
σ_a^g	Absorption cross section for group g , probability of a neutron in group g being absorbed (no neutron exiting after collision)
σ_f^g	Fission cross section for group g , probability of a neutron in group g having a fission collision
$\sigma_{P0}^{g \rightarrow g'}$	P0 scattering cross section for group g scattering to group g' , probability of a neutron scattering from group g to group g'
$\sigma_{P1}^{g \rightarrow g'}$	P1 scattering cross section from group g to group g' , anisotropic term to modify scattering angle from neutrons scattering from group g to group g'
ν^g	The number of neutrons produced (on average) due to a fission collision in group g
χ^g	Fission energy distribution for group g , the probability that a fission neutron is born in group g

The values in Table 4 are used during a multi-group calculation to sample what happens during a neutron transport calculation. The total cross section is used to determine

if a collision happens and then the other cross sections determine the result of that collision. The absorption, fission, and P0 cross sections are used to determine the reaction type for a given group with the total cross section in a group being defined as,

$$\sigma_t^g = \sigma_a^g + \sigma_f^g + \sum_{g'} \sigma_{P0}^{g \rightarrow g'} \quad (46)$$

Using the collision sampling method described in 3.2.6, the type of collision is determined. If absorption is sampled, then the neutron track is ended. If fission is sampled, then Equation 47 is used to sample how many neutrons are spawned from the reaction,

$$\# \text{ neutrons from fission} = \text{floor}(RN + \nu^g) \quad (47)$$

where RN is a random number on (0, 1). Equation 47 ensures that there is only an integer number of neutrons spawned from fission while preserving the average. For each of these neutrons spawned from fission, an energy group is assigned by sampling from the fission energy distribution χ^g . Since the $\sum_g \chi^g = 1$, the new energy group can be sampled the same as collisions are sampled in Figure 5. Each of these neutrons is then given a direction by sampling from an isotropic distribution. The neutron is assigned an angle using Equation 48 and 49 below,

$$\mu = 2 * RN - 1 \quad (48)$$

$$\varphi = 2\pi * RN \quad (49)$$

where RN is a random number on (0, 1), μ is the polar angle, and φ is the azimuthal angle. Here the polar angle is defined from the neutrons direction of travel. For scattering, the probability a neutron is assigned to a certain group is based off the scattering to a certain

group when compared to the total. So the probability of scattering from group g to a certain group g'' would be represented by Equation 50 below,

$$\frac{\sigma_{P0}^{g \rightarrow g''}}{\sum_{g'} \sigma_{P0}^{g \rightarrow g'}} \quad (50)$$

Using Equation 50, the probability of scattering from group g to every other group can be determined and thus sampled much like the fission exiting group or type of collision. In order to take into account anisotropy in the scattering cross sections, the P1 scattering cross section is used. The MORSE^[11] treatment of the P1 cross section is used in order to take into account this anisotropy. This treatment uses the following equation for determining the average scattering angle $\bar{\mu}$ from the P0 and P1 cross sections,

$$\bar{\mu} = \frac{\sigma_{P1}^{g \rightarrow g'}}{\sigma_{P0}^{g \rightarrow g'}} \quad (51)$$

The scattering angle is then set to the discrete $\bar{\mu}$ value, the same way as it is handled in MCNP^[12]. Finally, to sample the azimuthal angle out of the collision, Equation 49 is used.

3.2.8 Continuous energy formulation

A continuous energy representation of nuclear data aims to accurately represent the probabilities of various neutron interactions as faithfully as possible. There are many different nuclear datasets but one of the most detailed forms of data provided in the United States are the evaluated nuclear data files (ENDF)^[13]. These files are released by the Cross Section Evaluation Working Group and make use of both theory and experimental data to recreate nuclear data as closely as possible. These ENDF files are in the form of raw data that must be processed first in order to be used in neutron transport codes. Codes such as

NJOY^[14] and AMPX^[15] take the ENDF files and generate pointwise cross sections that recreate the nuclear data on a grid that can then be interpolated upon.

Determining the outcome of collisions for the continuous energy case is much like in the multi-group case except now the cross sections are often determined by interpolation. The continuous energy case is also able to account for many other reaction types such as (n, 2n), (n, He), (n, p), etc. From the nuclear data, cross sections for all of these reaction types can be obtained along with energy and angular distributions for the outgoing neutrons. SPaRC utilizes cross section data processed through the NJOY code system. MCNP also uses cross sections processed from NJOY, a detailed explanation of both how the data is formatted as well as how to correctly use the data can be found in the manual^[6]. In order to take into temperature effects, the cross sections utilized in SPaRC must be processed through NJOY at the appropriate temperature. At present SPaRC does not account for temperature if it differs than the specified nuclear data, but this is being investigated for future implementations.

3.2.9 Computing Responses

In neutron transport calculations, it is of importance to know what reactions of interest are occurring. In principle any value of the following form can be determined through the stochastic calculation,

$$T = \int \phi(E)f(E)dE \quad (52)$$

where $f(E)$ is often a cross section of interest. In order to approximate this integral SPaRC makes use of both collision and path length tallies.

Reaction rates can be estimated by recording values of interest when a particle makes a collision in a region. First a counter is implemented by using the following equation,

$$CT = CT + w \frac{\sigma_x}{\sigma_t} \quad (53)$$

where σ_x is the reaction of interest that is being estimated, and CT is the counter for that reaction. The reaction rate can then be estimated by normalizing by the source S , and volume ΔV , of the tally region of interest.

$$RR_{CT} = \frac{CT}{S\Delta V} \quad (54)$$

Then after the calculation is finished the counter is normalized to account for the number of source particles, volume, and energy domain. The result is a reaction rate per source (neutrons or neutrons per second), per unit energy, and per unit volume.

For optically thin regions where neutrons might not make many collisions, the path length estimator for tallies is a better option. This tally records results any time a neutron passes through a region and can be represented by the following equation,

$$PT = PT + w * p * \sigma_x \quad (55)$$

where PT is the path length counter and p is the distance traveled by the neutron in that region. Much like with the collision tally the reaction rate can be determined by normalizing by the source and volume,

$$RR_{PT} = \frac{PT}{S\Delta V} \quad (56)$$

For the tallies of interest for surface to volume responses in the SPaRC code, the path length formulation is used. For each incoming angular flux expansion, the reaction rate of

interest is recorded (e.g. fission), and then the total reaction rate is reconstructed at the end of the calculation once the coefficients for each of the expansions is determined.

3.2.10 Variance Reduction

Any stochastic calculation will have some variance associated with the solution. This variance can be reduced by simulating more particles, but unfortunately scales proportionally to the square root of the number of samples. In a physical experiment, if a neutron undergoes an absorption process the neutron disappears. During a simulation we can introduce a weight w , to a neutron and then modify that weight instead of terminating a neutron after an absorption reaction. When an absorption collision happens the neutron weight can be modified by the following equation,

$$w_{after} = w_{before} * (1 - \sigma_a / \sigma_t) \quad (57)$$

Not terminating the neutron if an absorption collision is sampled allows for the neutron to continue on and generate results of interest instead of just being terminated. Here for an absorption collision the weight of the particle is reduced by its absorption probability. In this way, the neutron survives to generate results while the weight is modified to correctly account for the absorption.

Particles with little or no weight will have little effect on generating tallies of interest. In order to not waste computational resources on these low weight particles a process known as Russian Roulette is performed. In this process, if a neutrons weight falls below a threshold value, a random number will be sampled to see if the neutron history gets terminated. If the random number sampled is less than the current weight of the neutron, the neutron weight is set to 1. Conversely, if the random number is above the current weight of the neutron, the neutron history is terminated.

For a more detailed survey of stochastic transport methods References 6, 10, and 16 provide a good start.

CHAPTER 4

SPARC IMPLEMENTATION DETAILS

The following chapter will detail some of the specifics involved with the SPaRC implementation for generating cross sections as well as the database management techniques. The various sampling techniques and procedures in Chapter 3 describe the theory behind the SPaRC implementation. This section will go into detail on some of the specifics of the implementation for use in COMET as opposed to general neutron transport.

4.1 Response Generation Implementation

The input for response generation and management consists of a main input file that details the main components of the calculation and then there are separate files for each coarse mesh detailing its geometry and materials. The following lists details the contents of the main input file:

- Run parameters – The number of particles to calculate each response is specified as well as how many times the response function calculation is split (for parallel calculation).
- Expansion orders – Sets the maximum orders of the position and angular expansions for response generation as well as the maximum order of the cross terms.
- Eigenvalue (k) grid – The number of eigenvalues and their values are specified at which responses are generated. It should be noted that multiple responses based on k are only needed in the case that a coarse mesh contains fissionable material.
- Random number generator seed – Number used to initialize the PRNG to allow for repeated runs. If no seed is given, the PRNG is initialized using a seed based off of the current time at calculation.

- Coarse mesh parameters – Lists the coarse meshes used in the problem, specifies the name of the file where the geometric and material properties are located and indicates whether or not the region contains a fissionable isotope for generating responses on a k-grid and for depletion calculations.
- Calculation type – Specifies either that the calculation is multi-group or continuous energy, and then specifies the number of groups (for a multi-group calculations) or the energy expansion on the surface in the continuous energy case.
- Depletion – Indicator as to whether this is a depletion calculation, and specifies the burnup points. Will lead to the creation of a response database for reactions important to depletion.
- Work directory – Specifies the location where responses will be outputted.
- Data directory – Specifies the location of the nuclear data.
- Symmetry – Indicates whether half, quarter, or no symmetry is able to be used for the generation of responses.

As indicated earlier, there are separate files containing the data specific to a unique coarse mesh. These files contain the following data:

- Geometry – Surfaces are specified that make up the problem. The first surface defined represents the coarse mesh boundary, then the rest of the surfaces are defined that compose the rest of the coarse mesh. The first surface is defined in such a way in order to set the surfaces that surface-to-surface responses are calculated from. This implementation is for Cartesian COMET so the coarse meshes are right parallelepipeds. New boundaries can be implemented to make use of other geometries such as hexagonal.
- Cells – For a given region the material is specified followed by the density in that region and then indicators as to whether the cell falls inside or outside a given surface as defined in the geometry section.

- Materials – The materials are indicated by giving the identifier to the cross section data and then specifying what atom percent of that material makes up the whole.
- Fuel – Specifies regions where there is fissionable material present. This indicator allows for the generation of production and fission density responses that are used for the deterministic calculations. If depletion is specified, the number of regions in which to track isotopics and reactions is also specified.

With these parameters from both the main input file and from the coarse mesh files, the response function parameters are fully defined. Response calculations are started by reading in the main input file and then generating a list of responses that need to be calculated. The number of responses are based off how many coarse meshes are specified, how many of those coarse meshes contain fissionable material, the size of the eigenvalue grid, and the symmetry specified. With the number of responses specified along with what responses need to be generated, the details of the coarse mesh are read in from its geometry file and the calculation begins. Calculations are started by spawning a neutron from the boundary of a coarse mesh and then tracking that neutron until it leaves the mesh and the surface-to-surface response is calculated. Along the way, responses are generated for production, depletion, etc. based off what was specified in the file. After the responses are generated, they are stored in a database format.

4.2 Database Management

For managing the response database, one of the key points to consider is that only surface-to-surface responses and the surface-to-volume neutron production responses are needed for the deterministic COMET calculations. These surface-to-surface responses are needed to update the coefficients during the inner iterations (Equation 20) and then the eigenvalue can be updated using the production and surface-to-surface responses (Equation 21). It should be noted that the absorption response in Equation 21 can be reconstructed

from the production and surface responses. Separate responses such as all of the reaction rates for various isotopes needed for depletion calculations can be stored in a separate database.

For a given coarse mesh, surface, and energy group, two separate binary database files are generated. The first binary database file contains the surface-to-surface and production responses needed for the COMET deterministic iterations while the second file contains all of the other responses of interest. For depletion calculations, this file contains the reaction rate responses for 10 different reactions and 300 different isotopes. The files have the same format of integer pointers followed by the response data in double format. The pointers for the first database contain the response expansion, orders, number of groups, surface, and eigenvalue while the pointers for the depletion database indicate the same values except with pointers for the number of reactions and isotopes to be tracked, as well as how many regions of the fuel are being depleted.

The database was formatted this way, with many separate binary files to allow for parallel computations for both the COMET deterministic calculations and the depletion calculations. This way data can be accessed from separate files without any competition conditions. The format is flexible enough to allow for changes in the data representation when developing this parallel capacity in the future.

4.3 Parallelization through the Message Passing Interface (MPI)

SPaRC makes use of parallel computing through the message passing interface (MPI). Since all of the neutron histories simulated for the response calculation are, in principle, independent of one another, the calculation can be parallelized almost arbitrarily up to the total number of neutrons simulated. The results of these parallel runs can then be combined at the end of the calculations to obtain a solution. For practical applications, it is not feasible to parallelize the calculation to that extent. The amount of parallelization used in the response calculations will be discussed after the parallel scheme is introduced.

A “master-slave” paradigm is used for the parallel computation. In this implementation, the master node performs all of the input, output, and combination of responses, while the slave nodes perform the transport calculations and generate the responses. For a given response generation calculation, the master node first reads the main input file and determined how many calculations are to be performed and splits the response generation tasks up to be sent out to the slave processes. The master node then reads in the coarse mesh geometry and the nuclear data used in the calculation and then sends the data out to each of the slave nodes. Finally, the master node sends out a response generation task to be completed to each of the slave nodes. These calculations are naturally split by surface, energy group, coarse mesh type, and eigenvalue but are further divided by specifying how many particles are used for each calculation. After the master node sends the task data, it waits until the slave processes complete their calculations. At the completion of the response generation, the slave node sends the data back to the master node where the response data is combined. The master node then sends the next task out to the slave node that just finished the calculation. Once the master node receives all of the response data for a specific calculation, the master node prints the response data out to a binary file and purges the data from memory. Once all of the tasks have been completed the master node signals the slave nodes to terminate the MPI process. Figure 6 shows a representation of the generation process.

When implementing parallel programs, it is of interest to know how the calculation speed scales with the number of processors. In theory, fixed source neutron transport should be perfectly scalable since the calculations are independent of one another. In practice however, time must be taken at both the beginning and end of the calculation to send out tasks and then combine the solutions. In order to test the scalability of the SPaRC code, a response calculation was run on a different number of nodes and the time to solution was recorded. The calculation involved the simulation of 10,000,000 particles per response with a (2 2 2 2) expansion order in space and angle for a 4 group energy structure. The

calculation involved the generation of 48 separate responses which can then be split further. If a response calculation is split 100 times, that equates to 4,800 separate response calculations. The calculations were run on a cluster with 112 processors. Table 5 gives the time for response generation based on the number of particles and how many times each response calculation is split.

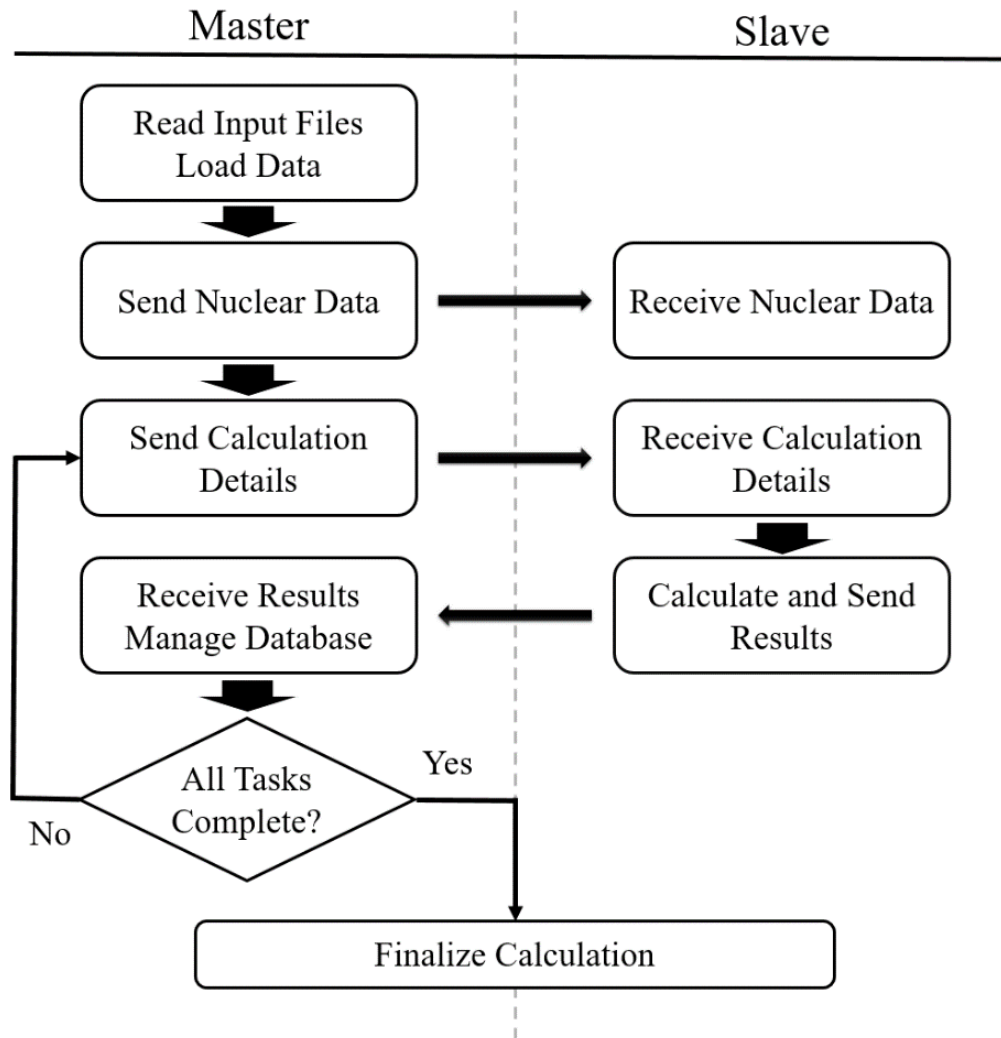


Figure 6. Parallelization of response calculation through the master-slave paradigm.

Table 5. Time to solution for response function generation using different parallelization schemes.

Processors	Number of times a response calculation is split					
	1	10	50	100	200	500
1	23347	23693	23361	23736	23629	24276
10	2971	2718	2688	2673	2707	2722
25	1036	1024	1013	1012	1016	1378
50	563	508	500	500	499	506
75	541	351	322	331	332	337
96	547	261	261	259	259	266
112	542	250	223	223	222	231

As seen in Table 5, it is important to split the response functions correctly in order to achieve the best time to solution. If the response function is split too many times, the communication time between the master and slave nodes increases and the time to solution also increases. However, if the response generation is not split enough times, there may not be enough different calculations to take advantage of the number of nodes available. In the extreme case of not splitting the response function calculations at all, no speedup is obtained for using any more processors after 49. This is because there are only 48 separate responses to be generated so there will be no work after all of the responses are being calculated. It is up to the user to specify how many times the response functions are split based upon the number of processes and the number of neutrons used for a calculation.

To show the scalability of the response function generation, the speedup and parallel efficiency obtained when increasing the number of processors was calculated using Equation 58 and 59.

$$speedup_n = \frac{t_1}{t_n} \quad (58)$$

$$parallel\ efficiency_n = \frac{speedup_n}{n} \quad (59)$$

where n is the number of processors used, t_1 is the time to solution when using one processor for the calculation and t_n is the time to solution for a calculation using n processors. Figure 7 shows the scalability of the response generation with the number of processors and Figure 8 shows the parallel efficiency. It is seen that SPaRC response generation scales well with around 95% parallel efficiency for calculations run on a 112 core cluster. The lower efficiency at a lower number of processors is related to the fact that the master node does not do any response generation but only updates the responses and performs I/O.

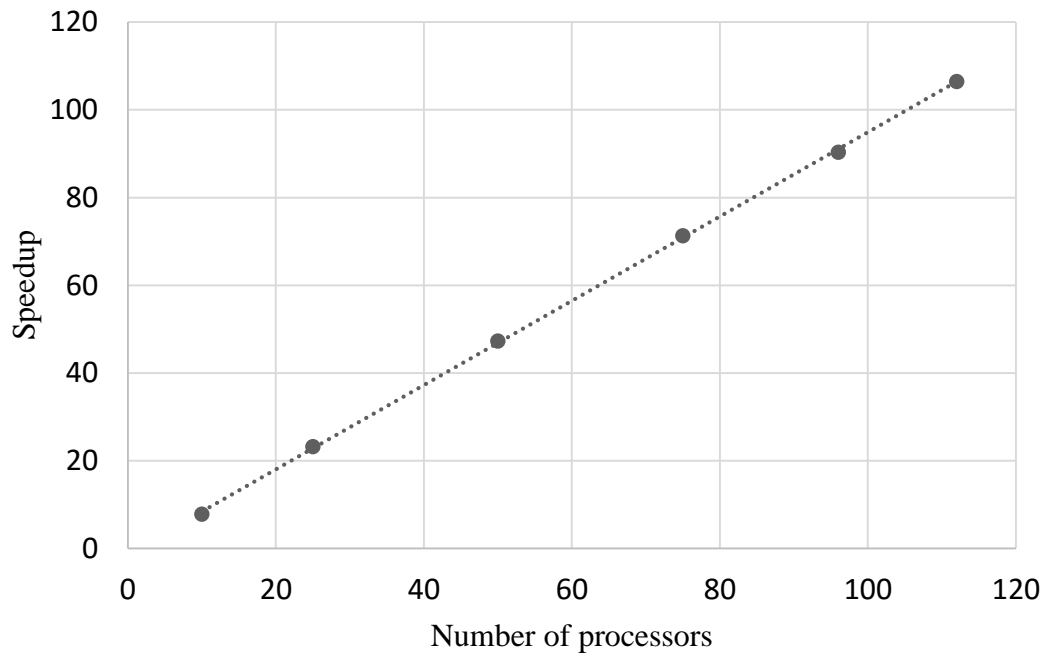


Figure 7. Parallel scaling of the response function generation.

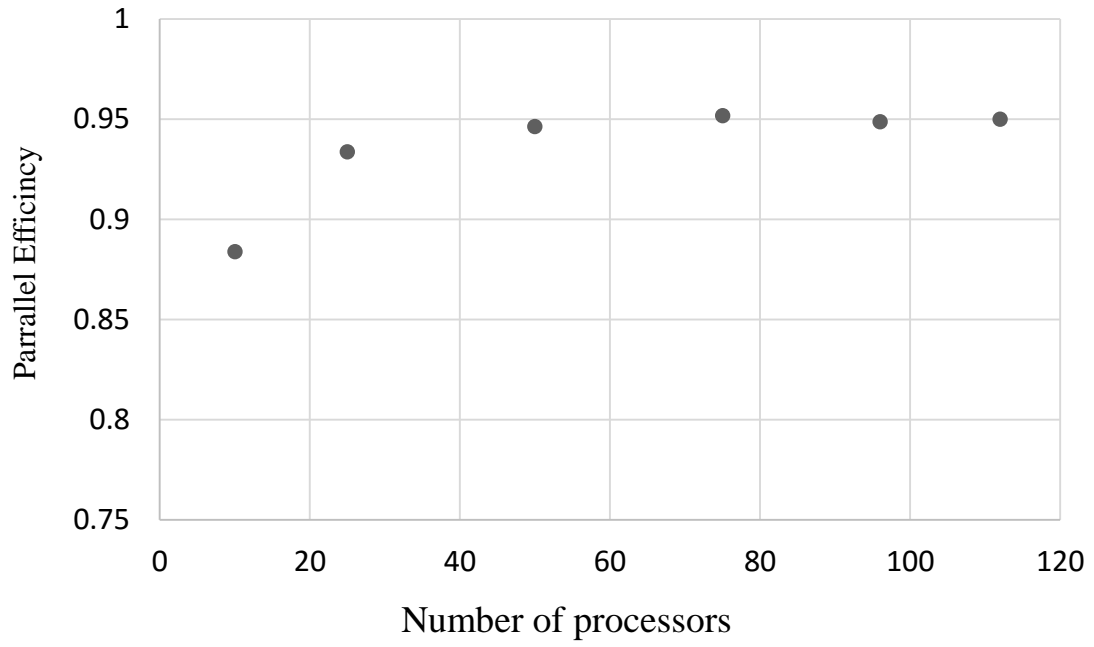


Figure 8. Parallel efficiency of the response generation.

CHAPTER 5

RESULTS

In order to test SPaRC, several neutronics benchmarks were created. Several fixed source “toy” benchmark problems were tested with MCNP and compared to SPaRC results. In addition, responses were generated with the previous COMET generation method and with the new SPaRC generation code. The results from the deterministic COMET iterations were then compared.

5.1 Fixed Source Benchmarking

In order to test the accuracy of SPaRC, multiple small-scale benchmark problems were developed. These benchmarks are similar in that they have very simple geometry, consisting of a couple of regions, and only a few unique materials. The simplicity of the benchmarks allows for comparisons to be made with other transport codes, by allowing for it to be easily seen if the codes treat the nuclear data or geometry differently. Results for the SPaRC code were tested against MCNP in order to validate the neutron transport routine. There were many benchmark cases that were investigated in order to test the transport code. These cases covered a range of different geometrical configurations as well as many different isotopes and used both multi-group and continuous energy data. The following is a list of some of the benchmarks cases tested:

1. A cube with 5cm sides with UO₂ fuel. The calculation was run with 8 energy groups with an isotropic point source at the center of the cube spawning neutrons in the 8th energy group.
2. A cylinder with a height of 5cm and a radius of 2.5cm with UO₂ fuel. The calculation was run with 47 energy groups with an isotropic point source at the center spawning neutrons in the 20th energy group.

3. A sphere with a radius of 5cm containing H^1 and the associated $S(\alpha,\beta)$ thermal file. The calculation is performed in continuous energy and the isotropic point source generates at the center generates neutrons at an energy of 0.1 MeV.
4. A sphere with a radius of 2.5cm containing U^{235} . The calculation is performed in continuous energy and the isotropic point source at the center generates neutrons at an energy of 0.1 MeV.
5. Fuel pin cell with materials and geometry as described for the uncontrolled assembly in 5.2.1. The calculation was run with continuous energy cross sections and the isotropic point source at the center generates neutrons at an energy of 0.01 MeV.

While the list is not inclusive of all the cases tested, it provides a good overview of the scope of tests. For each of the benchmark cases, Table 6 contains the calculated escape, absorption, and fission tallies normalized to a source particle for both SPaRC and MCNP calculations. The differences in SPaRC and MCNP results are shown in Table 7.

Table 6. Fixed source benchmark results for escape, absorption, and fission for MCNP and SPaRC.

Benchmark Case	MCNP			SPaRC		
	Escape	Absorption	Fission	Escape	Absorption	Fission
1	1.70120	0.19244	0.61602	1.70144	0.19246	0.61617
2	0.45735	0.62283	0.05530	0.45733	0.62294	0.05537
3	0.62625	0.37377	-	0.62592	0.37387	-
4	2.03710	0.14181	0.77392	2.05191	0.14269	0.77864
5	0.98385	0.01802	0.00132	0.98388	0.01802	0.00132

*Standard deviations $\sim 5e-4$

Table 7. Difference in fixed source benchmark results between MCNP and SPaRC.

Benchmark Case	Difference (%)		
	Escape	Absorption	Fission
1	0.01411	0.01195	0.02354
2	0.00459	0.01750	0.12856
3	0.05206	0.02595	-
4	0.72701	0.62337	0.61040
5	0.00285	0.00444	0.20942

The code was benchmarked for multiple isotopes and situations not listed in Table 6. However, these results are provided to show that for both multi-group and continuous energy fixed source calculations, the results generated from SPaRC and MCNP show excellent agreement (under 1% difference). For most of the cases, the differences between SPaRC and MCNP are within one standard deviation. There is only a significant difference in case 4 which contains U^{235} at an unphysical density of 25 g/cm³. This case, which is developed to introduce a case with a lot of fission, highlights the fact that fission is treated slightly differently between MCNP and SPaRC. However, the difference seen in case 4 is not seen in case 5 which contains U^{235} in a realistic nuclear fuel composition. Determining the source of this difference between the two codes is an area of future work.

Next, to benchmark the codes further within the COMET framework, an assembly benchmark will be introduced and eigenvalue and fission density responses will be compared from calculations using SPaRC and MCNP generated responses. Since a continuous energy version of COMET has not yet been developed, the results compared will be from multi-group calculations.

5.2 European Pressurized Reactor Benchmark

The European Pressurized Reactor or Evolutionary Power Reactor, now just EPR, is a commercial pressurized water reactor developed by AREVA^[17]. The reactor is a 4 loop PWR with 241 fuel assemblies laid out in a Cartesian grid and is designed to operate at 1,650 MWe. For benchmarking purposes, the assembly design for the EPR was stylized

and transformed for use as a benchmark problem. The dimensions of the assemblies found in Table 8 were taken from the design, as well as the control composition and the composition of the Gadded fuel rods. The UO₂ fuel pins have been modified from the EPR design to a higher enrichment and the cladding was changed to be natural zirconium. Lastly, values were assumed for the soluble boron concentration and for the temperatures and densities of all of the materials.

5.2.1 Assembly Specifications

Three separate assembly specifications were chosen in order to simulate a range of situations that may occur in a reactor core. The three assemblies include an uncontrolled case, a controlled case, and a gadded case. All three of these assemblies have pin cells laid out in a 17 x 17 Cartesian grid with 24 guide tubes/control rods and 265 pins containing fuel. The geometric parameters of the assembly are laid out in Table 8.

Table 8. EPR geometric assembly parameters

Fuel Rods	265	
Guide Tubes	24	
Pin Pitch	1.259840	cm
Cladding Outer Radius	0.474980	cm
Cladding Inner Radius	0.417957	cm
Fuel Pellet Radius	0.409575	cm
Guide Tube Outer Radius	0.622300	cm
Guide Tube Inner Radius	0.572770	cm
Control Cladding Outer Radius	0.433070	cm
Control Cladding Inner Radius	0.386080	cm
Absorber Outer Radius	0.381889	cm
Absorber Inner Radius	0.220980	cm

The uncontrolled assembly is made up of two unique pin cells a fuel pin cell and a guide tube cell. The fuel pin consists of UO₂ fuel with uranium enriched to 3.5 wt% U²³⁵

with the balance consisting of U^{238} . The fuel pin cell has cylindrical geometry with a central fuel region followed by a small voided gap, zirconium cladding, and then moderator surrounding the cladding. The pin cell geometry can be seen in Figure 8 (A). The guide tube cells consist of a cylindrical central moderator region followed by zirconium cladding and then more moderator on the outside of the cladding. The guide tube geometry can be seen in Figure 9 (B). Figure 10 shows the locations of the fuel and guide tube cells for the uncontrolled assembly. The controlled assembly has the same layout as the uncontrolled assembly, but the guide tubes now have control material inside them. The control material has an annular geometry with a central void and a small void between the control material and cladding and this all is located inside of the guide tube. Figure 8 (C) shows the control rod geometry.

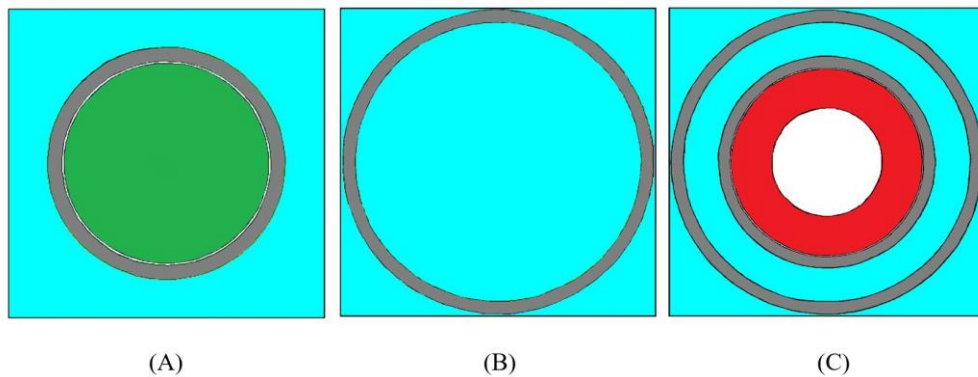


Figure 9. EPR assembly pin geometry for: (A) Fuel/Gadged Pin, (B) Guide Tube, (C) Guide Tube with Control Rod

The gaddled assembly is similar to the uncontrolled case except that 16 of the fuel pins have been replaced with pins that contain gadolinium. Of these 16 pins, 4 have 2 wt% gadolinium while 12 have 8 wt% gadolinium. These gadolinium fuel pins have the same geometry as the UO_2 fuel pins and are laid out in the assembly as shown in Figure 10.

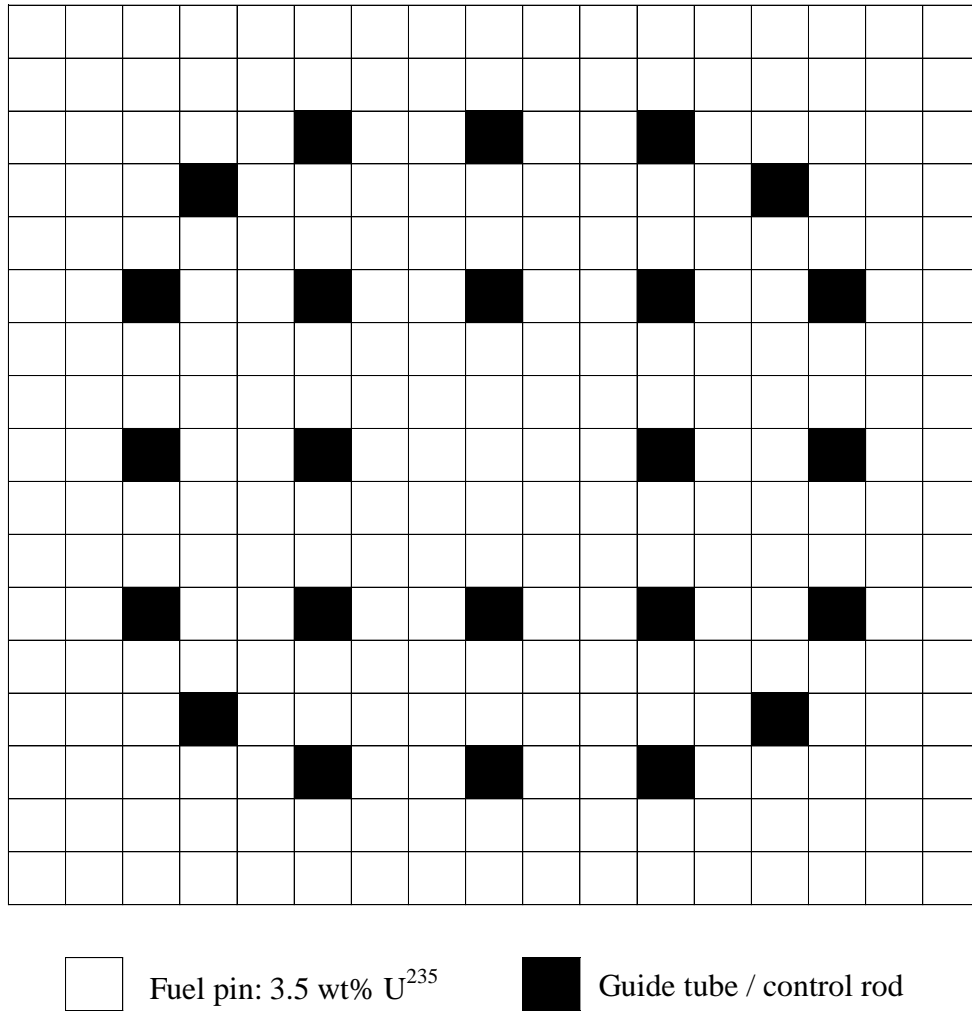


Figure 10. EPR uncontrolled/controlled assembly layout

The material compositions for the fuel, gadded fuel, cladding, and moderator are located in Table 9. The temperature of the fuel and gadded fuel is assumed to be 900K while everything else (the moderator and cladding) is assumed to be 600K.

Table 9. EPR material compositions

Material	Composition	Density	Details
Fuel	UO ₂	10.4 g/cm ³	Uranium is 3.5 wt% U ²³⁵ and 96.5 wt% U ²³⁸
2% Gd Fuel	UO ₂ & Gd ₂ O ₃	10.4 g/cm ³	Gd composes 2 wt% of the fuel, the uranium is 3 wt% U ²³⁵ and 97 wt% U ²³⁸
8% Gd Fuel	UO ₂ & Gd ₂ O ₃	10.4 g/cm ³	Gd composes 8 wt% of the fuel, the uranium is 2.27 wt% U ²³⁵ and 97.73 wt% U ²³⁸
Cladding	Natural Zr	6.514 g/cm ³	-
Moderator	H ₂ O & Natural B	0.7 g/cm ³	1000 ppm boron

Table 10. EPR assembly temperatures

Fuel Temperature	900 K
Moderator/Structure Temperature	600 K

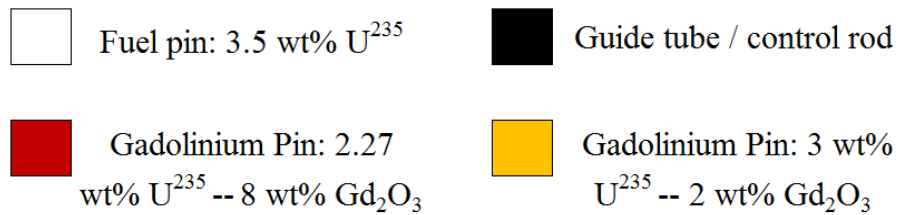
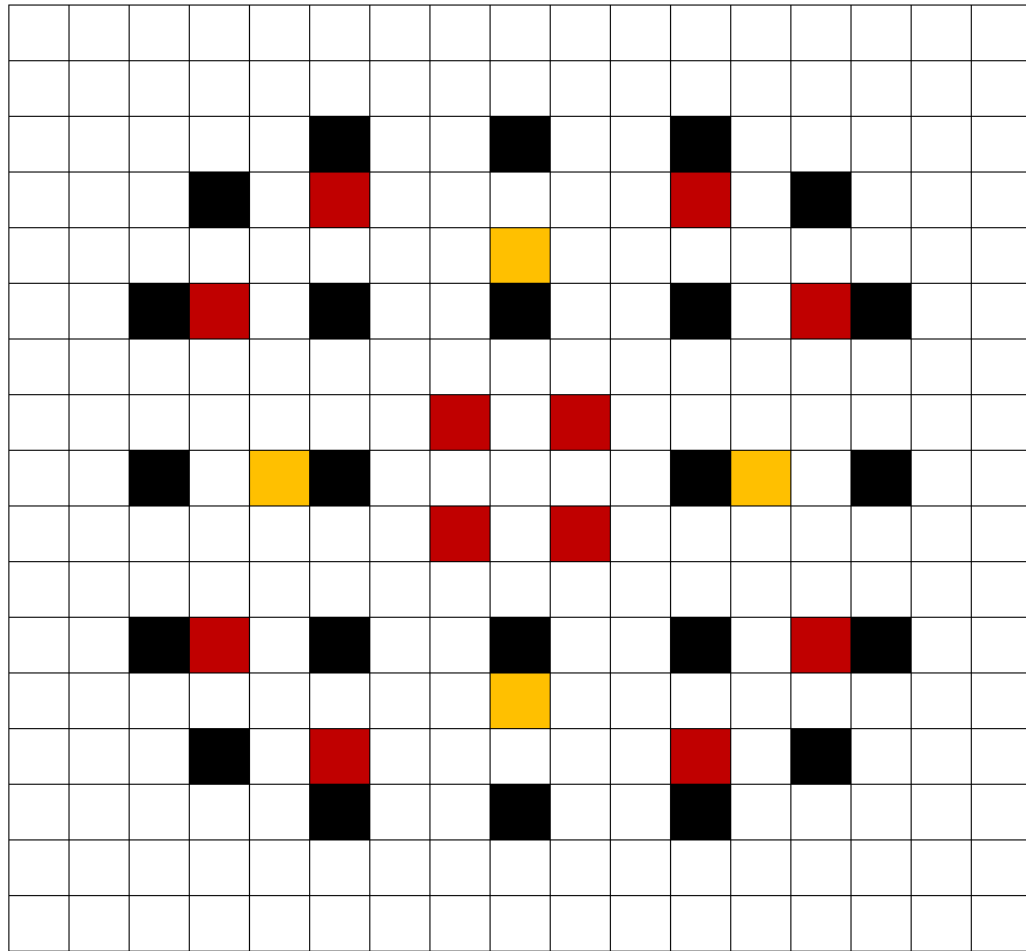


Figure 11. EPR gaddled assembly layout.

5.2.2 HELIOS Nuclear Data Generation

In order to generate multi-group nuclear data for use in response generation, HELIOS^[18] version 1.10 was used. HELIOS is an advanced lattice depletion code that utilizes method of characteristics (MOC) and collision probability (CPM) solvers in 2D general geometry. The code has been widely used and verified for the development of

nuclear data libraries for both light and heavy water reactors. The uncontrolled, controlled, and gadded assemblies as defined in section 5.2.1 were modeled in HELIOS utilizing the 1/8th symmetry of the assemblies. The transport mesh used for the three assemblies can be seen in Figure 12, 13, and 14. The calculations were performed using the 190 group adjusted library provided by HELIOS and cross sections were outputted for each unique material in an assembly in 2, 4, and 8 energy groups. The energy group structure for 2, 4, and 8 groups is shown in Table 11. The cross sections generated for the uncontrolled assembly include a fuel, moderator, and cladding cross section. For the uncontrolled assembly, fuel, moderator, cladding, and absorber cross sections were generated. Finally, for the gadded assembly there are cross sections for the fuel, 2% gadolinium fuel, 8% gadolinium fuel, cladding, and moderator. The nuclear data provided include the total, absorption, P0 and P1 cross sections and if the material is fissionable, the fission cross section is provided along with the fission spectrum and the number of neutrons emitted from fission. These cross sections were used to generate responses in the following sections and are provided in Appendix B so that the reader can recreate the calculations performed.

Table 11. Energy group structure for cross section generation.

Two Group	Four Group	Eight Group	Lower Energy Bound (eV)
		1	2.2313E+06
	1	2	8.2085E+05
		3	9.1188E+03
1		4	1.3007E+02
	2	5	3.9279E+00
	3	6	6.2506E-01
		7	1.4572E-01
2	4	8	1.0000E-04

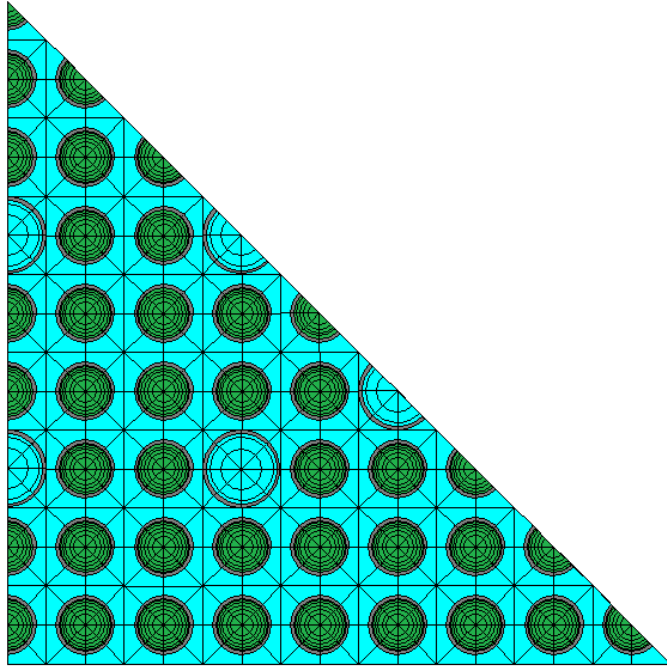


Figure 12. HELIOS model of the uncontrolled 17x17 EPR assembly.

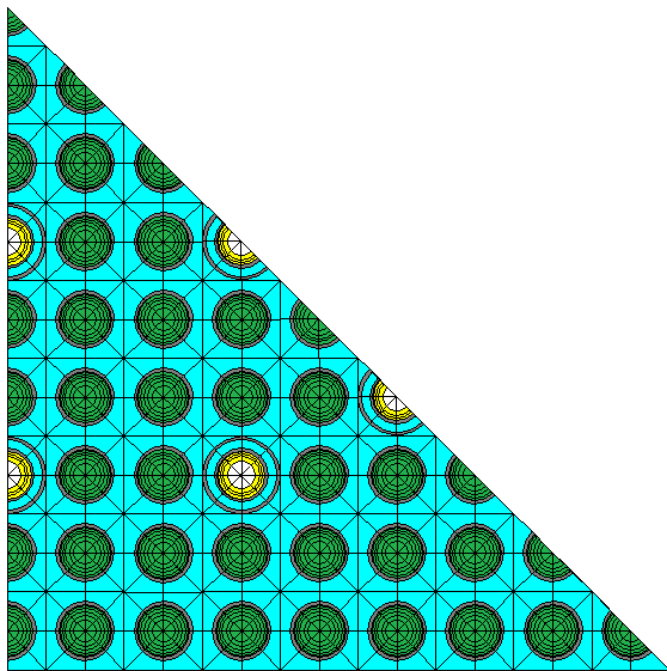


Figure 13. HELIOS model of the controlled 17x17 EPR assembly.

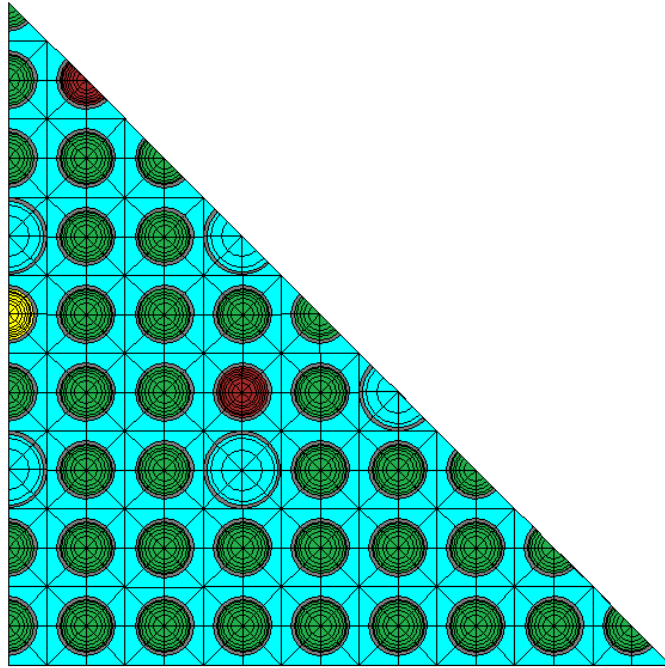


Figure 14. HELIOS model of the 17x17 gaddened EPR assembly.

5.2.3 COMET Response Calculations

The uncontrolled, controlled, and gaddened assemblies were solved using the COMET methodology. For the calculations, unique pin cells were set to be the coarse meshes. This meant that the deterministic COMET calculations for the assemblies consisted of iterating on the responses of a 17 x 17 grid of pin coarse meshes as laid out in Figure 10 and 11. For the uncontrolled assembly there are two unique coarse meshes, a fuel pin mesh and a guide tube mesh. The controlled assembly similarly has two coarse meshes, a fuel and a control rod coarse mesh. The gaddened assembly has 4 unique coarse meshes namely, a fuel pin, guide tube, 2% gadolinium fuel pin, and 8% gadolinium fuel pin. The list of coarse meshes for the assembly types can be found in Table 12, 13, and 14.

Table 12. Uncontrolled assembly coarse meshes.

Coarse Mesh	Description
1	Fuel pin
2	Guide tube

Table 13. Controlled assembly coarse meshes

Coarse Mesh	Description
1	Fuel pin
2	Control rod

Table 14. Gadded assembly coarse meshes.

Coarse Mesh	description
1	Fuel Pin
2	Guide Tube
3	2% Gd Fuel Pin
4	8% Gd Fuel Pin

For each of these coarse meshes, responses were generated using the multi-group cross sections generated in section 5.2.2. In order to benchmark the new response generation method, responses were generated with both MCNP and SPaRC. The surface-to-surface and surface-to-volume responses were then compared between the two generation methods. Next, the two sets of responses were used to generate both eigenvalue and fission results with COMET. These eigenvalue and fission density results were also compared for the uncontrolled, controlled, and gadded cases.

For the analysis of fission densities, the relative difference between the two solutions in a pin i can be introduced as follows,

$$RD_i = \frac{FD_i - FD_i^{ref}}{FD_i^{ref}} \quad (60)$$

where FD_i^{ref} is the reference solution fission density and FD_i is the calculated fission density. In order to compare the fission densities in an assembly, the average, max, and mean relative differences for the pin fission densities can be calculated using Equation 61, 62 and 63.

$$AVG = \frac{\sum_i |RE_i|}{N} \quad (61)$$

$$MAX = \max_i RE_i \quad (62)$$

$$MRD = \frac{\sum_i |RE_i| * FD_i}{N * FD_{avg}} \quad (63)$$

Responses for the three assemblies were performed with MCNP and SPaRC in two energy groups for expansion orders up to (2244), second order in the special variables, and fourth order in the angular variables. The average, maximum, and mean relative differences between the responses for each of the unique coarse meshes are given in Table 15, 16, 19, 20, 23, 24, 25, and 26. The differences from the COMET eigenvalues for the three assemblies can be found in Table 17, 21, and 27 while the pin fission density differences can be found in Table 18, 22, and 28.

5.2.4 Uncontrolled Assembly Results

The uncontrolled assembly consists of a fuel pin coarse mesh and a guide tube coarse mesh. Responses were calculated for these coarse meshes with both MCNP and SPaRC and the responses were compared. The responses were also used to generate assembly level results with COMET. The normalized fission density distribution calculated by COMET can be seen in Figure 15. It can be seen that the fission density is highest around the guide tubes where neutrons are thermalized.

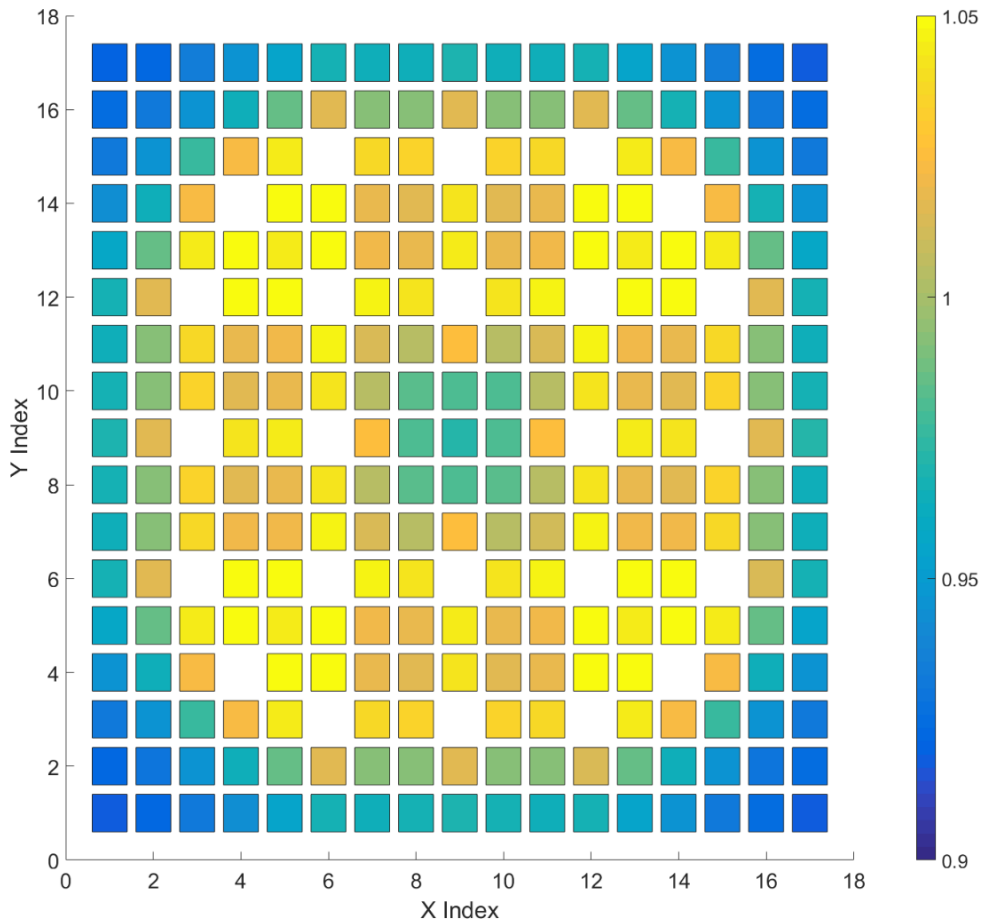


Figure 15. Uncontrolled assembly pin fission density.

Table 15. Difference between MCNP and SPaRC response functions for the fuel pin coarse mesh in the uncontrolled assembly case.

Response Type	Difference Between MCNP and SPaRC for Fuel Pin Responses					
	AVG (%)	Standard Deviation	MAX (%)	Standard Deviation	MRD (%)	Standard Deviation
Surface-to-surface	0.0495	3.708E-04	0.3162	3.503E-07	0.0121	4.193E-07
Surface-to-volume	0.0246	9.462E-08	0.0252	9.894E-08	0.0243	3.477E-06

As seen in Table 15 and 16, the responses calculated with both MCNP and SPaRC for the uncontrolled case agree very well. While the maximum error may seem high at 0.3%, this maximum value is seen at responses of very low magnitude. This effect is characterized by the mean relative error which weights the differences between the MCNP and SPaRC generated responses by their magnitude. For both the fuel pin and guide tube responses, the mean relative difference is very low, indicating that the SPaRC and MCNP agree well when calculating the responses that will have the most impact on the solution to the problem.

Table 16. Difference between MCNP and SPaRC surface-to-surface response functions for the guide tube coarse mesh in the uncontrolled assembly case.

Response Type	Difference Between MCNP and SPaRC for Fuel Pin Responses					
	AVG (%)	Standard Deviation	MAX (%)	Standard Deviation	MRD (%)	Standard Deviation
Surface-to-surface	0.0508	3.731E-04	0.1580	1.191E-06	0.0102	3.760E-07

Table 17 shows the COMET eigenvalue results for the uncontrolled assembly using responses generated with MCNP and SPaRC. The results were generated for a number of

different expansion orders and there was found to be good agreement. It was also found that the agreement in the pin powers was very good as seen in Table 18.

Table 17. COMET eigenvalue results and standard deviations for the uncontrolled EPR assembly with responses generated by both MCNP and SPaRC.

Expansion	MCNP	Standard Deviation (pcm)	SPaRC	Standard Deviation (pcm)	Diff (pcm)	Standard Deviation (pcm)
0000	1.24954	4.8	1.24968	4.8	14.6	6.73
2200	1.24575	4.7	1.24590	4.7	14.6	6.71
0022	1.24908	4.8	1.24923	4.8	14.9	6.73
2222	1.24576	4.8	1.24591	4.8	15	6.72
2244	1.24554	4.8	1.24569	4.9	15	6.81

Table 18. Difference in COMET pin powers for the uncontrolled EPR assembly with responses generated by both MCNP and SPaRC.

Expansion	AVG (%)	Standard Deviation	MAX (%)	Standard Deviation	MRD (%)	Standard Deviation
0000	1.15E-03	2.99E-04	3.10E-03	3.23E-05	1.14E-03	3.66E-04
2200	1.50E-03	3.00E-04	4.28E-03	4.58E-05	1.49E-03	3.70E-04
0022	2.54E-03	2.96E-04	2.54E-03	4.55E-05	9.14E-04	3.63E-04
2222	1.58E-03	3.02E-04	4.10E-03	4.81E-05	1.57E-03	3.73E-04
2244	1.49E-03	3.03E-04	4.15E-03	4.81E-05	1.49E-03	3.75E-04

For the uncontrolled assembly case the results obtained from COMET using the MCNP and SPaRC responses agree very well. Next, results will be presented for both the controlled and gadded assembly cases.

5.2.5 Controlled Assembly Results

The controlled assembly contains a fuel pin and control rod coarse mesh. Table 19, 20, 21 and 22 detail the differences between the MCNP and SPaRC generated results for the controlled assembly. The fission density distribution can be seen in Figure 16 with the fission density depressed around the control rod locations where neutrons are being absorbed.

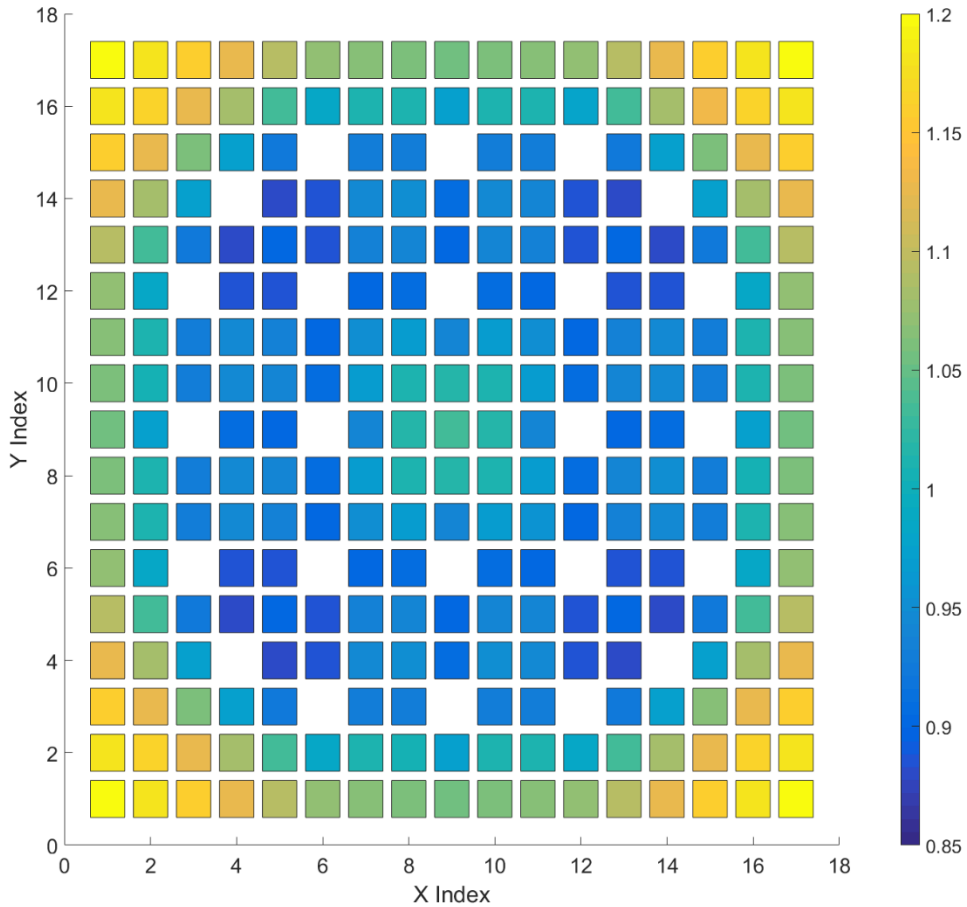


Figure 16. Controlled assembly pin fission density.

Table 19. Difference between MCNP and SPaRC response functions for the fuel pin coarse mesh in the controlled assembly case.

Response Type	Difference Between MCNP and SPaRC for Fuel Pin Responses					
	AVG (%)	Standard Deviation	MAX (%)	Standard Deviation	MRD (%)	Standard Deviation
Surface-to-surface	0.1145	9.147E-04	0.3732	3.072E-05	0.0190	9.076E-07
Surface-to-volume	0.0243	3.475E-07	0.0250	3.732E-07	0.0240	3.438E-06

The fuel pin responses for the controlled case show similar agreement to that of the uncontrolled case but, as seen in Table 20, the control rod response shows slightly larger differences. The largest difference, 1.6885% occurs in a response from the lowest energy group of the incoming response to the highest energy group of the outgoing response. For a control rod mesh, the absorption probability of low energy neutrons is very high, leading to very small responses from the lowest energy group to the highest group. The largest differences are once again seen in very small responses leading the mean relative difference to still be very small.

Table 20. Difference between MCNP and SPaRC response functions for the control rod coarse mesh in the controlled assembly case.

Response Type	Difference Between MCNP and SPaRC for Fuel Pin Responses					
	AVG (%)	Standard Deviation	MAX (%)	Standard Deviation	MRD (%)	Standard Deviation
Surface-to-surface	0.4669	1.767E-03	1.6885	1.478E-05	0.0036	9.515E-07

Table 21. COMET eigenvalue results and standard deviations for the controlled EPR assembly with responses generated by both MCNP and SPaRC.

Expansion	MCNP	Standard Deviation (pcm)	SPaRC	Standard Deviation (pcm)	Diff (pcm)	Standard Deviation (pcm)
0000	0.92382	3.6	0.92430	11.3	47.78	11.86
2200	0.93837	3.6	0.93887	11.5	49.62	12.08
0022	0.91228	3.5	0.91275	11.1	46.23	11.66
2222	0.91264	3.5	0.91310	11.1	45.1	11.67
2244	0.91254	3.5	0.91300	11.1	45.47	11.68

The eigenvalue results for the uncontrolled assembly case are detailed in Table 21. The differences between the eigenvalues are slightly larger than the uncontrolled case, at around 50 pcm, but are still very similar. As seen in Table 22, the fission density distribution generated from the SPaRC and MCNP responses agree very well.

Table 22. Difference in COMET pin powers for the controlled EPR assembly with responses generated with both MCNP and SPaRC.

Expansion	AVG (%)	Standard Deviation	MAX (%)	Standard Deviation	MRD (%)	Standard Deviation
0000	3.19E-03	5.46E-04	9.45E-03	9.89E-05	3.10E-03	7.58E-04
2200	3.43E-03	5.56E-04	9.61E-03	8.64E-05	3.42E-03	7.81E-04
0022	7.30E-03	5.44E-04	1.80E-02	8.23E-05	7.34E-03	7.48E-04
2222	8.70E-03	5.74E-04	2.15E-02	1.01E-04	8.79E-03	7.93E-04
2244	8.68E-03	5.76E-04	2.22E-02	9.94E-05	8.76E-03	7.96E-04

5.2.6 Gadded Assembly Results

The gadded assembly contains the most unique coarse meshes with a fuel pin, 2% gadolinium fuel pin, 8% gadolinium fuel pin, and guide tube coarse mesh. Table 23, 24, 25, 26, 27 and 28 detail the differences between SPaRC and MCNP calculations and the fission density distribution can be seen in Figure 17. In Figure 17 it can be seen that the fission density is lowest in and around the fuel pins containing the gadolinium absorber.

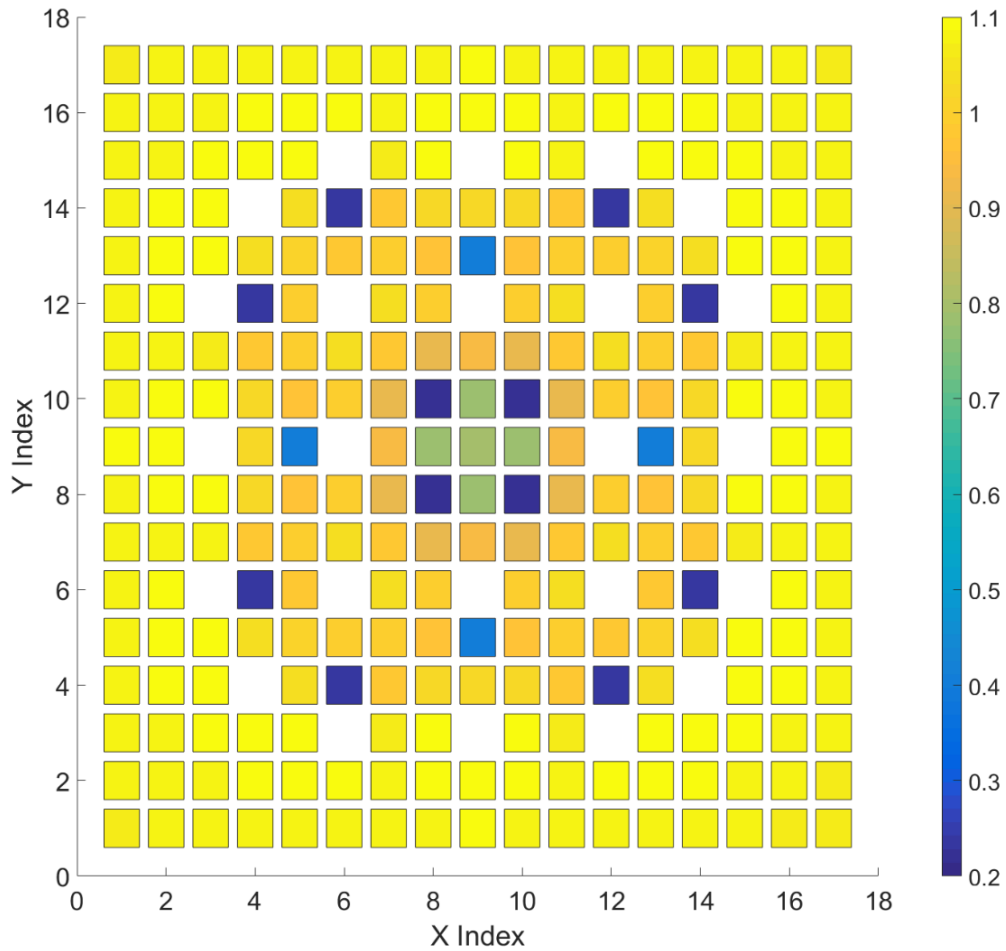


Figure 17. Gadded assembly pin fission.

Table 23. Difference between MCNP and SPaRC response functions for the fuel pin coarse mesh in the gadded assembly case.

Response Type	Difference Between MCNP and SPaRC for Fuel Pin Responses					
	AVG (%)	Standard Deviation	MAX (%)	Standard Deviation	MRD (%)	Standard Deviation
Surface-to-surface	0.0691	7.731E-04	0.2206	7.876E-06	0.0357	3.386E-06
Surface-to-volume	0.0146	1.596E-06	0.0170	1.267E-06	0.0146	4.132E-06

Table 24. Difference between MCNP and SPaRC response functions for the guide tube coarse mesh in the gadded assembly case.

Response Type	Difference Between MCNP and SPaRC for Fuel Pin Responses					
	AVG (%)	Standard Deviation	MAX (%)	Standard Deviation	MRD (%)	Standard Deviation
Surface-to-surface	0.1034	9.102E-04	0.3322	1.287E-06	0.0302	2.899E-06

Table 25. Difference between MCNP and SPaRC response functions for the 2% gadolinium fuel pin coarse mesh in the gadded assembly case.

Response Type	Difference Between MCNP and SPaRC for Fuel Pin Responses					
	AVG (%)	Standard Deviation	MAX (%)	Standard Deviation	MRD (%)	Standard Deviation
Surface-to-surface	0.0779	7.294E-04	0.4397	3.055E-06	0.0300	2.029E-06
Surface-to-volume	0.0013	9.305E-08	0.0015	7.882E-08	0.0012	3.667E-07

Table 26. Difference between MCNP and SPaRC response functions for the 8% gadolinium fuel pin coarse mesh in the gadded assembly case.

Response Type	Difference Between MCNP and SPaRC for Fuel Pin Responses					
	AVG (%)	Standard Deviation	MAX (%)	Standard Deviation	MRD (%)	Standard Deviation
Surface-to-surface	0.5269	8.578E-04	4.6922	1.356E-05	0.0466	1.786E-06
Surface-to-volume	0.0186	1.391E-07	0.0235	1.398E-07	0.0135	6.742E-06

Table 27. COMET eigenvalue results and standard deviations for the gadded EPR assembly with responses generated by both MCNP and SPaRC.

Expansion	MCNP	Standard Deviation (pcm)	SPaRC	Standard Deviation (pcm)	Diff (pcm)	Standard Deviation (pcm)
0000	1.07772	12.9	1.07822	13.0	50.3	18.32
2200	1.08756	13.1	1.08806	13.1	48.9	18.53
0022	1.06637	12.8	1.06686	12.8	48.3	18.06
2222	1.06599	12.8	1.06644	12.8	45	18.08
2244	1.06594	12.8	1.06639	12.8	44.1	18.08

Table 23, 24, 25, 26, 27 and 28 detail the results obtained from the gadded assembly response and COMET calculations. The response results are all very similar with a notable difference in the 8% gadolinium fuel responses. For this case the maximum difference is 4.7% occurring in responses from the lower energy group to the upper energy group like the controlled case. Since gadolinium is a strong neutron absorber these responses are also very small leading to large percent errors. The eigenvalue and pin fission density results are similar for both the MCNP and SPaRC responses.

Table 28. Difference in COMET pin powers for the gadded EPR assembly with responses generated with both MCNP and SPaRC.

Expansion	AVG (%)	Standard Deviation	MAX (%)	Standard Deviation	MRD (%)	Standard Deviation
0000	8.59E-03	7.07E-04	5.30E-02	2.31E-05	6.77E-03	9.03E-04
2200	1.46E-02	7.17E-04	7.15E-02	2.01E-05	1.24E-02	9.26E-04
0022	1.25E-02	7.04E-04	4.97E-02	2.14E-05	1.15E-02	8.96E-04
2222	1.56E-02	7.29E-04	5.71E-02	2.44E-05	1.46E-02	9.34E-04
2244	1.61E-02	7.36E-04	6.01E-02	2.46E-05	1.50E-02	9.41E-04

Responses for the different EPR assembly types have been generated with both the old MCNP response generator and the new SPaRC generator. It was found that there is good agreement between both the responses themselves and the eigenvalue and pin power distributions from the COMET deterministic calculations. The detailed pin fission density distributions and uncertainties can be found in Appendix B. There is a slight difference between the SPaRC and MCNP responses in all cases and the COMET eigenvalue with SPaRC responses is greater than the MCNP eigenvalue for all of the cases. The source of this difference is under investigation.

CHAPTER 6

CONCLUSION

A new code SPaRC has been developed for the generation of response functions for the COMET method. The new code provides this response function generation to facilitate further multi-physics calculations in the future. The transport routine has been validated against MCNP for both multi-group and continuous energy calculations with good results. It was also seen that the responses generated with SPaRC and MCNP agree well as well as the COMET eigenvalue and fission densities generated from those responses. Along with the response generation, database generation routines have also been developed. The response database has been split into separate binary files to both permit parallel deterministic COMET calculations and to separate out depletion data not needed during the deterministic iterations. The response generation has been implemented in parallel and the response function database has been developed with parallel computation in mind.

Future work includes incorporating SPaRC into a multi-physics code based on the COMET method, determining how to treat the energy variable on the boundaries of a coarse mesh for continuous energy calculations, and performing lattice depletion calculations. The code has been developed in order to easily facilitate the development of these new capabilities.

APPENDIX A

FISSION DENSITY DISTRIBUTION PLOTS

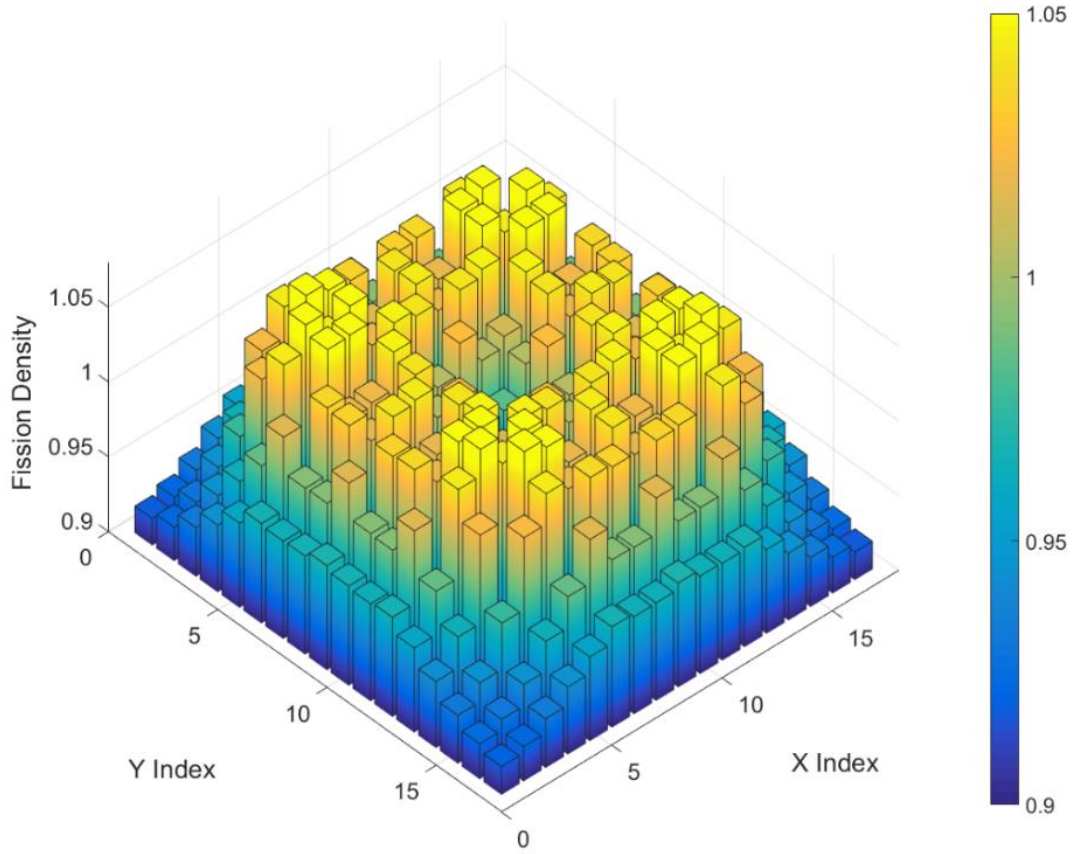


Figure 18. Fission density for the uncontrolled assembly.

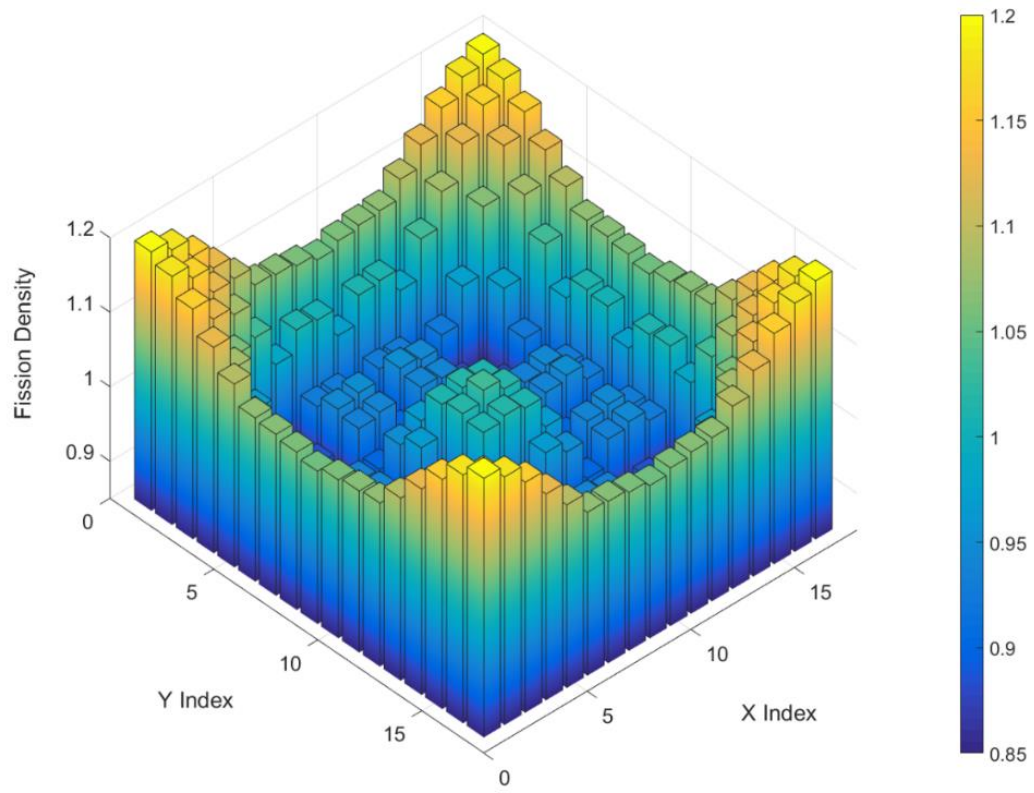


Figure 19. Fission density for the controlled assembly.

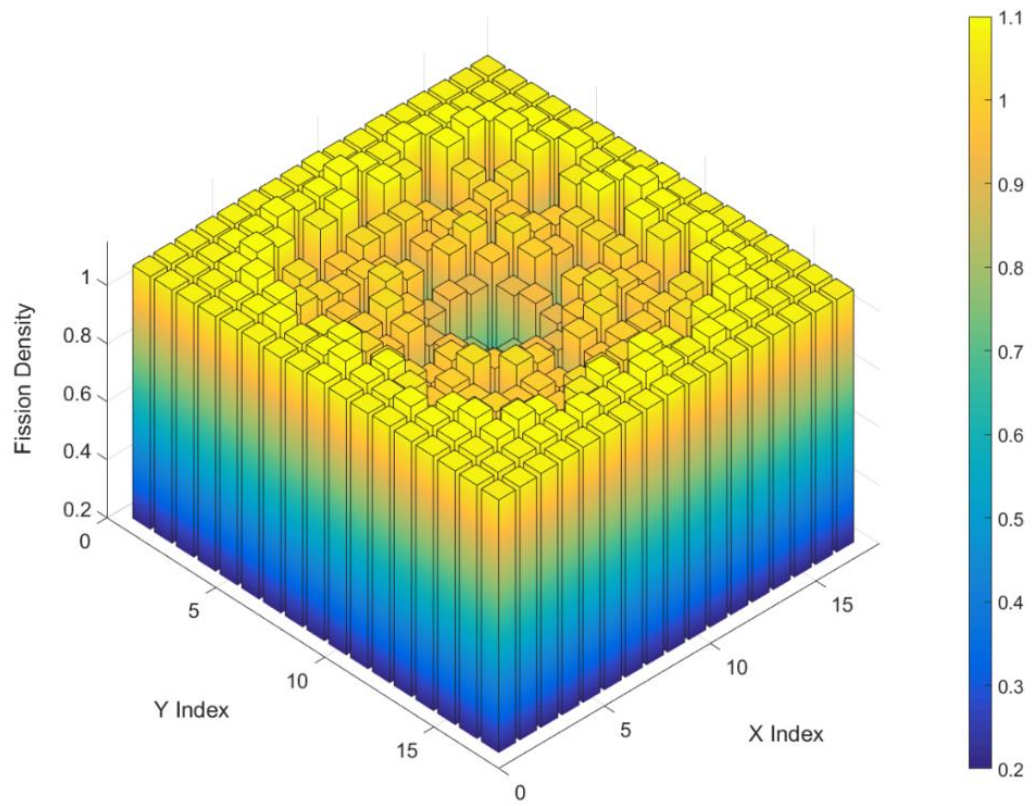


Figure 20. Fission density for the gaddled assembly.

APPENDIX B

MULTI-GROUP CROSS SECTIONS

A library of multi-group cross sections has been generated for uncontrolled, controlled, and gadded EPR assemblies using the lattice depletion transport code HELIOS version 1.10. These cross sections were then used to generate many of the results presented in this paper. To enable the reader to conduct their own calculations consistent with the calculations done in this paper, cross sections are provided in 2, 4, and 8 groups for the uncontrolled, controlled, and gadded assembly types. These cross sections are provided for each unique material in an assembly and are formatted as follows,

$$\left\{ \left\{ \sigma_{ag} \right\}_{g=1}^G, \left\{ \sigma_{fg} \right\}_{g=1}^G, \left\{ \nu_g \right\}_{g=1}^G, \left\{ \chi_g \right\}_{g=1}^G, \left\{ \left\{ \left\{ \sigma_{sn}^{g' \rightarrow g} \right\}_{g'=1}^G \right\}_{g=1}^G \right\}_{n=0}^N \right\}$$

where for G energy groups

σ_{ag} = group g absorption cross section

σ_{fg} = group g fission cross section

ν_g = group g fission yield

χ_g = fission spectrum corresponding to group g

$\sigma_{sn}^{g' \rightarrow g}$ = n 'th (of N) Legendre moment of the scattering cross section from g' to group g .

The cross sections that follow are organized first by assembly, then by group structure, and finally by material. Further details into the generation of these cross sections can be found in chapter 4 under the HELIOS benchmark results and nuclear generation section.

Uncontrolled EPR Assembly Cross Sections

The following are the cross sections for the uncontrolled EPR assembly. Cross sections are provided for the three unique regions namely, the UO₂ fuel, the zirconium cladding, and the moderator.

2 Group Cross Sections

Fuel

3.0293E-02	2.8822E-01	9.3919E-03	2.1950E-01	2.5380E+00	2.4338E+00
1.0000E+00	0.0000E+00	3.9581E-01	1.8739E-03	8.4189E-04	4.0549E-01
4.4424E-02	-1.7301E-04	-1.9530E-04	8.8885E-03		

Cladding

1.7498E-03	4.0983E-03	0.0000E+00	0.0000E+00	0.0000E+00	0.0000E+00
0.0000E+00	0.0000E+00	3.1380E-01	8.0584E-04	2.9605E-04	2.7446E-01
3.8125E-02	-9.9772E-05	-6.9536E-05	2.5442E-03		

Moderator

6.7210E-04	2.3682E-02	0.0000E+00	0.0000E+00	0.0000E+00	0.0000E+00
0.0000E+00	0.0000E+00	6.0397E-01	2.2208E-03	2.7435E-02	1.7642E+00
3.5983E-01	1.3819E-03	8.1001E-03	5.2031E-01		

4 Group Cross Sections

Fuel

8.4556E-03	8.1685E-02	4.9477E-02	2.8822E-01	4.8602E-03	1.6654E-02
3.0061E-02	2.1950E-01	2.7308E+00	2.4338E+00	2.4338E+00	2.4338E+00

9.9980E-01	1.9568E-04	0.0000E+00	0.0000E+00	3.5527E-01	0.0000E+00
0.0000E+00	0.0000E+00	1.6005E-03	4.9558E-01	0.0000E+00	0.0000E+00
0.0000E+00	2.4333E-03	3.7848E-01	1.8739E-03	0.0000E+00	0.0000E+00
1.5425E-02	4.0549E-01	6.1728E-02	0.0000E+00	0.0000E+00	0.0000E+00
4.9116E-04	9.1447E-03	0.0000E+00	0.0000E+00	0.0000E+00	-7.3792E-04
1.2274E-02	-1.7301E-04	0.0000E+00	0.0000E+00	-3.5782E-03	8.8885E-03

Cladding

5.7640E-04	4.7147E-03	1.0506E-03	4.0983E-03	0.0000E+00	0.0000E+00
0.0000E+00	0.0000E+00	0.0000E+00	0.0000E+00	0.0000E+00	0.0000E+00
0.0000E+00	0.0000E+00	0.0000E+00	0.0000E+00	3.0971E-01	0.0000E+00
0.0000E+00	0.0000E+00	5.4409E-04	3.3077E-01	0.0000E+00	0.0000E+00
0.0000E+00	6.2623E-04	2.6882E-01	8.0584E-04	0.0000E+00	0.0000E+00
5.2893E-03	2.7446E-01	5.5984E-02	0.0000E+00	0.0000E+00	0.0000E+00
-1.3859E-04	2.6486E-03	0.0000E+00	0.0000E+00	0.0000E+00	-2.0566E-04
3.6354E-03	-9.9772E-05	0.0000E+00	0.0000E+00	-1.2423E-03	2.5442E-03

Moderator

1.5728E-04	7.9994E-04	6.0137E-03	2.3682E-02	0.0000E+00	0.0000E+00
0.0000E+00	0.0000E+00	0.0000E+00	0.0000E+00	0.0000E+00	0.0000E+00
0.0000E+00	0.0000E+00	0.0000E+00	0.0000E+00	3.5581E-01	0.0000E+00
0.0000E+00	0.0000E+00	6.1525E-02	9.3777E-01	0.0000E+00	0.0000E+00
1.9635E-05	8.5712E-02	6.8330E-01	2.2208E-03	1.2992E-06	1.5988E-02
4.0293E-01	1.7642E+00	2.0735E-01	0.0000E+00	0.0000E+00	0.0000E+00
2.6898E-02	5.9344E-01	0.0000E+00	0.0000E+00	0.0000E+00	4.0408E-02

4.5466E-01	1.3819E-03	0.0000E+00	2.7844E-03	1.2860E-01	5.2031E-01
------------	------------	------------	------------	------------	------------

8 Group Cross Sections

Fuel

1.4562E-02	8.1888E-03	6.5013E-03	3.8748E-02	1.5132E-01	4.9477E-02
1.7601E-01	3.8033E-01	1.3543E-02	6.2266E-03	1.2677E-03	8.0553E-03
3.0600E-02	3.0061E-02	1.3141E-01	2.9181E-01	2.8825E+00	2.6120E+00
2.4507E+00	2.4338E+00	2.4338E+00	2.4338E+00	2.4338E+00	2.4338E+00
3.5053E-01	4.1072E-01	2.3856E-01	1.9568E-04	0.0000E+00	0.0000E+00
0.0000E+00	0.0000E+00	1.7493E-01	0.0000E+00	0.0000E+00	0.0000E+00
0.0000E+00	0.0000E+00	0.0000E+00	0.0000E+00	3.6057E-02	2.3750E-01
0.0000E+00	0.0000E+00	0.0000E+00	0.0000E+00	0.0000E+00	0.0000E+00
2.2578E-02	5.8717E-02	4.2420E-01	0.0000E+00	0.0000E+00	0.0000E+00
0.0000E+00	0.0000E+00	9.3657E-06	7.1143E-06	2.8847E-03	5.0986E-01
0.0000E+00	0.0000E+00	0.0000E+00	0.0000E+00	2.9926E-25	0.0000E+00
2.1172E-25	5.2518E-03	4.6387E-01	0.0000E+00	0.0000E+00	0.0000E+00
0.0000E+00	0.0000E+00	0.0000E+00	0.0000E+00	6.3799E-03	3.7848E-01
4.1565E-03	0.0000E+00	0.0000E+00	0.0000E+00	0.0000E+00	0.0000E+00
0.0000E+00	1.5425E-02	3.6655E-01	2.8801E-02	0.0000E+00	0.0000E+00
0.0000E+00	0.0000E+00	0.0000E+00	0.0000E+00	3.1973E-02	3.8240E-01
9.7380E-02	0.0000E+00	0.0000E+00	0.0000E+00	0.0000E+00	0.0000E+00
0.0000E+00	0.0000E+00	-3.8468E-04	7.3095E-02	0.0000E+00	0.0000E+00
0.0000E+00	0.0000E+00	0.0000E+00	0.0000E+00	2.9523E-04	-1.0583E-02
4.9256E-02	0.0000E+00	0.0000E+00	0.0000E+00	0.0000E+00	0.0000E+00
3.9937E-07	0.0000E+00	-8.8737E-04	1.0018E-02	0.0000E+00	0.0000E+00

0.0000E+00	0.0000E+00	0.0000E+00	0.0000E+00	0.0000E+00	-1.6104E-03
1.0339E-02	0.0000E+00	0.0000E+00	0.0000E+00	0.0000E+00	0.0000E+00
0.0000E+00	0.0000E+00	-1.9348E-03	1.2274E-02	-3.8376E-04	0.0000E+00
0.0000E+00	0.0000E+00	0.0000E+00	0.0000E+00	0.0000E+00	-3.5779E-03
1.4370E-02	-4.8472E-03	0.0000E+00	0.0000E+00	0.0000E+00	0.0000E+00
0.0000E+00	-2.7551E-07	-5.1652E-03	1.3476E-02		

Cladding

7.9172E-05	4.9487E-04	7.8107E-04	7.5568E-03	2.6954E-04	1.0506E-03
2.5006E-03	5.3250E-03	0.0000E+00	0.0000E+00	0.0000E+00	0.0000E+00
0.0000E+00	0.0000E+00	0.0000E+00	0.0000E+00	0.0000E+00	0.0000E+00
0.0000E+00	0.0000E+00	0.0000E+00	0.0000E+00	0.0000E+00	0.0000E+00
0.0000E+00	0.0000E+00	0.0000E+00	0.0000E+00	0.0000E+00	0.0000E+00
0.0000E+00	0.0000E+00	1.1833E-01	0.0000E+00	0.0000E+00	0.0000E+00
0.0000E+00	0.0000E+00	0.0000E+00	0.0000E+00	3.4604E-02	2.2795E-01
0.0000E+00	0.0000E+00	0.0000E+00	0.0000E+00	0.0000E+00	0.0000E+00
2.0523E-02	1.5877E-02	3.8579E-01	0.0000E+00	0.0000E+00	0.0000E+00
0.0000E+00	0.0000E+00	3.1313E-07	0.0000E+00	9.7681E-04	3.6861E-01
0.0000E+00	0.0000E+00	0.0000E+00	0.0000E+00	0.0000E+00	0.0000E+00
0.0000E+00	1.2578E-03	2.6962E-01	0.0000E+00	0.0000E+00	0.0000E+00
0.0000E+00	0.0000E+00	0.0000E+00	0.0000E+00	1.6057E-03	2.6882E-01
1.8553E-03	0.0000E+00	0.0000E+00	0.0000E+00	0.0000E+00	0.0000E+00
0.0000E+00	5.2893E-03	2.5849E-01	9.6352E-03	0.0000E+00	0.0000E+00
0.0000E+00	0.0000E+00	0.0000E+00	0.0000E+00	1.4151E-02	2.6623E-01
5.3510E-02	0.0000E+00	0.0000E+00	0.0000E+00	0.0000E+00	0.0000E+00

0.0000E+00	0.0000E+00	-4.7573E-04	7.9668E-02	0.0000E+00	0.0000E+00
0.0000E+00	0.0000E+00	0.0000E+00	0.0000E+00	-1.2522E-05	-7.2424E-04
4.6438E-02	0.0000E+00	0.0000E+00	0.0000E+00	0.0000E+00	0.0000E+00
0.0000E+00	0.0000E+00	-2.4884E-04	3.1395E-03	0.0000E+00	0.0000E+00
0.0000E+00	0.0000E+00	0.0000E+00	0.0000E+00	0.0000E+00	-4.1295E-04
2.5267E-03	0.0000E+00	0.0000E+00	0.0000E+00	0.0000E+00	0.0000E+00
0.0000E+00	0.0000E+00	-5.2732E-04	3.6354E-03	-2.2971E-04	0.0000E+00
0.0000E+00	0.0000E+00	0.0000E+00	0.0000E+00	0.0000E+00	-1.2423E-03
5.4484E-03	-1.7412E-03	0.0000E+00	0.0000E+00	0.0000E+00	0.0000E+00
0.0000E+00	0.0000E+00	-2.7036E-03	4.1314E-03		

Moderator

7.7378E-04	4.2560E-06	1.9970E-05	2.5280E-04	1.6405E-03	6.0137E-03
1.4252E-02	3.0657E-02	0.0000E+00	0.0000E+00	0.0000E+00	0.0000E+00
0.0000E+00	0.0000E+00	0.0000E+00	0.0000E+00	0.0000E+00	0.0000E+00
0.0000E+00	0.0000E+00	0.0000E+00	0.0000E+00	0.0000E+00	0.0000E+00
0.0000E+00	0.0000E+00	0.0000E+00	0.0000E+00	0.0000E+00	0.0000E+00
0.0000E+00	0.0000E+00	5.8890E-02	0.0000E+00	0.0000E+00	0.0000E+00
0.0000E+00	0.0000E+00	0.0000E+00	0.0000E+00	4.8423E-02	1.1710E-01
0.0000E+00	0.0000E+00	0.0000E+00	0.0000E+00	0.0000E+00	0.0000E+00
2.6426E-02	1.2258E-01	4.8313E-01	0.0000E+00	0.0000E+00	0.0000E+00
0.0000E+00	0.0000E+00	2.9100E-04	1.2284E-03	1.0799E-01	8.1980E-01
0.0000E+00	0.0000E+00	0.0000E+00	0.0000E+00	0.0000E+00	9.8440E-06
1.4938E-03	2.0679E-01	8.0133E-01	0.0000E+00	0.0000E+00	0.0000E+00
0.0000E+00	0.0000E+00	3.5151E-05	5.3516E-03	2.0916E-01	6.8330E-01

5.2226E-03	0.0000E+00	0.0000E+00	0.0000E+00	2.3258E-06	7.7636E-04
2.9943E-02	3.3466E-01	8.9215E-01	1.8966E-01	0.0000E+00	0.0000E+00
0.0000E+00	2.1470E-04	9.0852E-03	6.8265E-02	4.5850E-01	1.8804E+00
3.3549E-02	0.0000E+00	0.0000E+00	0.0000E+00	0.0000E+00	0.0000E+00
0.0000E+00	0.0000E+00	3.1465E-02	6.3946E-02	0.0000E+00	0.0000E+00
0.0000E+00	0.0000E+00	0.0000E+00	0.0000E+00	9.3931E-03	5.6494E-02
2.9147E-01	0.0000E+00	0.0000E+00	0.0000E+00	0.0000E+00	0.0000E+00
8.7307E-06	7.4025E-05	4.8039E-02	5.3881E-01	0.0000E+00	0.0000E+00
0.0000E+00	0.0000E+00	0.0000E+00	0.0000E+00	7.8210E-05	9.2966E-02
5.3454E-01	0.0000E+00	0.0000E+00	0.0000E+00	0.0000E+00	0.0000E+00
0.0000E+00	4.7294E-04	1.0176E-01	4.5466E-01	3.2499E-03	0.0000E+00
0.0000E+00	0.0000E+00	0.0000E+00	2.0943E-05	6.2338E-03	1.2340E-01
4.7244E-01	3.4210E-02	0.0000E+00	0.0000E+00	0.0000E+00	0.0000E+00
7.9591E-04	5.2035E-03	6.6815E-02	4.7208E-01		

Controlled Assembly Cross Sections

The following are the cross sections for the controlled EPR assembly. Cross sections are provided for the four unique regions namely, the UO₂ fuel, the zirconium cladding, the moderator, and the absorber material in the control rod.

2 Group Cross Sections

Fuel

2.9111E-02	2.7851E-01	9.0524E-03	2.1196E-01	2.5429E+00	2.4338E+00
1.0000E+00	0.0000E+00	3.9495E-01	2.3385E-03	7.0748E-04	4.0465E-01

4.5079E-02 -2.1306E-04 -1.6440E-04 8.9366E-03

Cladding

1.7552E-03 3.9476E-03 0.0000E+00 0.0000E+00 0.0000E+00 0.0000E+00

0.0000E+00 0.0000E+00 3.1535E-01 1.0402E-03 2.4593E-04 2.7416E-01

3.8641E-02 -1.2842E-04 -5.7803E-05 2.5783E-03

Moderator

6.1750E-04 2.2816E-02 0.0000E+00 0.0000E+00 0.0000E+00 0.0000E+00

0.0000E+00 0.0000E+00 6.0540E-01 2.8308E-03 2.4128E-02 1.7259E+00

3.6009E-01 1.7660E-03 7.0438E-03 5.2170E-01

Absorber

1.6558E-01 7.5004E+00 0.0000E+00 0.0000E+00 0.0000E+00 0.0000E+00

0.0000E+00 0.0000E+00 3.3121E-01 2.2696E-03 1.2388E-04 2.5886E-01

5.9967E-02 0.0000E+00 0.0000E+00 2.0060E-03

4 Group Cross Sections

Fuel

8.4277E-03 7.9953E-02 4.9041E-02 2.7851E-01 4.8422E-03 1.6416E-02

2.9657E-02 2.1196E-01 2.7294E+00 2.4338E+00 2.4338E+00 2.4338E+00

9.9980E-01 1.9568E-04 0.0000E+00 0.0000E+00 3.5512E-01 0.0000E+00

0.0000E+00 0.0000E+00 1.5816E-03 4.9642E-01 0.0000E+00 0.0000E+00

0.0000E+00 2.2148E-03 3.7883E-01 2.3385E-03 0.0000E+00 0.0000E+00

1.4949E-02 4.0465E-01 6.1761E-02 0.0000E+00 0.0000E+00 0.0000E+00

-4.8541E-04 9.0782E-03 0.0000E+00 0.0000E+00 0.0000E+00 -6.7152E-04

1.2162E-02	-2.1306E-04	0.0000E+00	0.0000E+00	-3.4736E-03	8.9366E-03
------------	-------------	------------	------------	-------------	------------

Cladding

5.8071E-04	4.7735E-03	1.0426E-03	3.9476E-03	0.0000E+00	0.0000E+00
0.0000E+00	0.0000E+00	0.0000E+00	0.0000E+00	0.0000E+00	0.0000E+00
0.0000E+00	0.0000E+00	0.0000E+00	0.0000E+00	3.1113E-01	0.0000E+00
0.0000E+00	0.0000E+00	5.4669E-04	3.3193E-01	0.0000E+00	0.0000E+00
0.0000E+00	5.6151E-04	2.6899E-01	1.0402E-03	0.0000E+00	0.0000E+00
5.1175E-03	2.7416E-01	5.5958E-02	0.0000E+00	0.0000E+00	0.0000E+00
-1.3925E-04	2.6354E-03	0.0000E+00	0.0000E+00	0.0000E+00	-1.8440E-04
3.5885E-03	-1.2842E-04	0.0000E+00	0.0000E+00	-1.2028E-03	2.5783E-03

Moderator

1.5001E-04	7.7638E-04	5.9711E-03	2.2816E-02	0.0000E+00	0.0000E+00
0.0000E+00	0.0000E+00	0.0000E+00	0.0000E+00	0.0000E+00	0.0000E+00
0.0000E+00	0.0000E+00	0.0000E+00	0.0000E+00	3.5952E-01	0.0000E+00
0.0000E+00	0.0000E+00	6.2569E-02	9.4258E-01	0.0000E+00	0.0000E+00
1.9963E-05	8.1448E-02	6.8824E-01	2.8308E-03	1.3194E-06	1.5201E-02
3.9735E-01	1.7259E+00	2.0965E-01	0.0000E+00	0.0000E+00	0.0000E+00
2.7341E-02	5.9588E-01	0.0000E+00	0.0000E+00	0.0000E+00	3.7968E-02
4.5754E-01	1.7660E-03	0.0000E+00	2.6153E-03	1.2631E-01	5.2170E-01

Absorber

1.5159E-02	3.1354E-01	2.7791E+00	7.5004E+00	0.0000E+00	0.0000E+00
0.0000E+00	0.0000E+00	0.0000E+00	0.0000E+00	0.0000E+00	0.0000E+00

0.0000E+00	0.0000E+00	0.0000E+00	0.0000E+00	3.1930E-01	0.0000E+00
0.0000E+00	0.0000E+00	5.5317E-04	3.7231E-01	0.0000E+00	0.0000E+00
0.0000E+00	1.9301E-04	2.0981E-01	2.2696E-03	0.0000E+00	0.0000E+00
4.8754E-03	2.5886E-01	8.3770E-02	0.0000E+00	0.0000E+00	0.0000E+00
0.0000E+00	2.9737E-03	0.0000E+00	0.0000E+00	0.0000E+00	0.0000E+00
1.5551E-03	0.0000E+00	0.0000E+00	0.0000E+00	0.0000E+00	2.0060E-03

8 Group Cross Sections

Fuel

1.4556E-02	8.1900E-03	6.4706E-03	3.8552E-02	1.5013E-01	4.9041E-02
1.7209E-01	3.7977E-01	1.3536E-02	6.2282E-03	1.2647E-03	8.0191E-03
3.0650E-02	2.9657E-02	1.2851E-01	2.9137E-01	2.8809E+00	2.6120E+00
2.4510E+00	2.4338E+00	2.4338E+00	2.4338E+00	2.4338E+00	2.4338E+00
3.5053E-01	4.1072E-01	2.3856E-01	1.9568E-04	0.0000E+00	0.0000E+00
0.0000E+00	0.0000E+00	1.7468E-01	0.0000E+00	0.0000E+00	0.0000E+00
0.0000E+00	0.0000E+00	0.0000E+00	0.0000E+00	3.6144E-02	2.3744E-01
0.0000E+00	0.0000E+00	0.0000E+00	0.0000E+00	0.0000E+00	0.0000E+00
2.2601E-02	5.8696E-02	4.2359E-01	0.0000E+00	0.0000E+00	0.0000E+00
0.0000E+00	0.0000E+00	9.2849E-06	7.1124E-06	2.8443E-03	5.0963E-01
0.0000E+00	0.0000E+00	0.0000E+00	0.0000E+00	2.9690E-25	0.0000E+00
2.1521E-25	5.1650E-03	4.6528E-01	0.0000E+00	0.0000E+00	0.0000E+00
0.0000E+00	0.0000E+00	0.0000E+00	0.0000E+00	5.9691E-03	3.7883E-01
4.7958E-03	0.0000E+00	0.0000E+00	0.0000E+00	0.0000E+00	0.0000E+00
0.0000E+00	1.4949E-02	3.6870E-01	2.9115E-02	0.0000E+00	0.0000E+00
0.0000E+00	0.0000E+00	0.0000E+00	0.0000E+00	2.9068E-02	3.8208E-01

9.7299E-02	0.0000E+00	0.0000E+00	0.0000E+00	0.0000E+00	0.0000E+00
0.0000E+00	0.0000E+00	-3.9346E-04	7.3071E-02	0.0000E+00	0.0000E+00
0.0000E+00	0.0000E+00	0.0000E+00	0.0000E+00	2.9595E-04	-1.0557E-02
4.9455E-02	0.0000E+00	0.0000E+00	0.0000E+00	0.0000E+00	0.0000E+00
3.9532E-07	0.0000E+00	-8.7506E-04	9.9926E-03	0.0000E+00	0.0000E+00
0.0000E+00	0.0000E+00	0.0000E+00	0.0000E+00	0.0000E+00	-1.5863E-03
1.0217E-02	0.0000E+00	0.0000E+00	0.0000E+00	0.0000E+00	0.0000E+00
0.0000E+00	0.0000E+00	-1.8098E-03	1.2162E-02	-4.3695E-04	0.0000E+00
0.0000E+00	0.0000E+00	0.0000E+00	0.0000E+00	0.0000E+00	-3.4733E-03
1.4049E-02	-4.8708E-03	0.0000E+00	0.0000E+00	0.0000E+00	0.0000E+00
0.0000E+00	-2.6659E-07	-4.7888E-03	1.3499E-02		

Cladding

8.2289E-05	4.9489E-04	7.7965E-04	7.5195E-03	2.6514E-04	1.0426E-03
2.4507E-03	5.3075E-03	0.0000E+00	0.0000E+00	0.0000E+00	0.0000E+00
0.0000E+00	0.0000E+00	0.0000E+00	0.0000E+00	0.0000E+00	0.0000E+00
0.0000E+00	0.0000E+00	0.0000E+00	0.0000E+00	0.0000E+00	0.0000E+00
0.0000E+00	0.0000E+00	0.0000E+00	0.0000E+00	0.0000E+00	0.0000E+00
0.0000E+00	0.0000E+00	1.1834E-01	0.0000E+00	0.0000E+00	0.0000E+00
0.0000E+00	0.0000E+00	0.0000E+00	0.0000E+00	3.4604E-02	2.2816E-01
0.0000E+00	0.0000E+00	0.0000E+00	0.0000E+00	0.0000E+00	0.0000E+00
2.0572E-02	1.5881E-02	3.8561E-01	0.0000E+00	0.0000E+00	0.0000E+00
0.0000E+00	0.0000E+00	3.1634E-07	0.0000E+00	9.6863E-04	3.6861E-01
0.0000E+00	0.0000E+00	0.0000E+00	0.0000E+00	0.0000E+00	0.0000E+00
0.0000E+00	1.2288E-03	2.6969E-01	0.0000E+00	0.0000E+00	0.0000E+00

0.0000E+00	0.0000E+00	0.0000E+00	0.0000E+00	1.4834E-03	2.6899E-01
2.1850E-03	0.0000E+00	0.0000E+00	0.0000E+00	0.0000E+00	0.0000E+00
0.0000E+00	5.1175E-03	2.5974E-01	9.8485E-03	0.0000E+00	0.0000E+00
0.0000E+00	0.0000E+00	0.0000E+00	0.0000E+00	1.2558E-02	2.6601E-01
5.3491E-02	0.0000E+00	0.0000E+00	0.0000E+00	0.0000E+00	0.0000E+00
0.0000E+00	0.0000E+00	-4.8532E-04	7.9755E-02	0.0000E+00	0.0000E+00
0.0000E+00	0.0000E+00	0.0000E+00	0.0000E+00	-1.1908E-05	-7.3094E-04
4.6522E-02	0.0000E+00	0.0000E+00	0.0000E+00	0.0000E+00	0.0000E+00
0.0000E+00	0.0000E+00	-2.4675E-04	3.1298E-03	0.0000E+00	0.0000E+00
0.0000E+00	0.0000E+00	0.0000E+00	0.0000E+00	0.0000E+00	-4.0343E-04
2.4861E-03	0.0000E+00	0.0000E+00	0.0000E+00	0.0000E+00	0.0000E+00
0.0000E+00	0.0000E+00	-4.8715E-04	3.5885E-03	-2.6976E-04	0.0000E+00
0.0000E+00	0.0000E+00	0.0000E+00	0.0000E+00	0.0000E+00	-1.2028E-03
5.1996E-03	-1.7745E-03	0.0000E+00	0.0000E+00	0.0000E+00	0.0000E+00
0.0000E+00	0.0000E+00	-2.4152E-03	4.1656E-03		

Moderator

7.6570E-04	4.2470E-06	1.9968E-05	2.5167E-04	1.6195E-03	5.9711E-03
1.3980E-02	3.0539E-02	0.0000E+00	0.0000E+00	0.0000E+00	0.0000E+00
0.0000E+00	0.0000E+00	0.0000E+00	0.0000E+00	0.0000E+00	0.0000E+00
0.0000E+00	0.0000E+00	0.0000E+00	0.0000E+00	0.0000E+00	0.0000E+00
0.0000E+00	0.0000E+00	0.0000E+00	0.0000E+00	0.0000E+00	0.0000E+00
0.0000E+00	0.0000E+00	5.8780E-02	0.0000E+00	0.0000E+00	0.0000E+00
0.0000E+00	0.0000E+00	0.0000E+00	0.0000E+00	4.8590E-02	1.1700E-01
0.0000E+00	0.0000E+00	0.0000E+00	0.0000E+00	0.0000E+00	0.0000E+00

2.6510E-02	1.2324E-01	4.8347E-01	0.0000E+00	0.0000E+00	0.0000E+00
0.0000E+00	0.0000E+00	2.9196E-04	1.2338E-03	1.0783E-01	8.2146E-01
0.0000E+00	0.0000E+00	0.0000E+00	0.0000E+00	0.0000E+00	9.9184E-06
1.4917E-03	2.0510E-01	8.0763E-01	0.0000E+00	0.0000E+00	0.0000E+00
0.0000E+00	0.0000E+00	3.5086E-05	5.3085E-03	2.0380E-01	6.8824E-01
6.0694E-03	0.0000E+00	0.0000E+00	0.0000E+00	2.3189E-06	7.7010E-04
2.9191E-02	3.2996E-01	9.0075E-01	1.9104E-01	0.0000E+00	0.0000E+00
0.0000E+00	2.1279E-04	8.8566E-03	6.7383E-02	4.3745E-01	1.8737E+00
3.3481E-02	0.0000E+00	0.0000E+00	0.0000E+00	0.0000E+00	0.0000E+00
0.0000E+00	0.0000E+00	3.1586E-02	6.3860E-02	0.0000E+00	0.0000E+00
0.0000E+00	0.0000E+00	0.0000E+00	0.0000E+00	9.4298E-03	5.6770E-02
2.9166E-01	0.0000E+00	0.0000E+00	0.0000E+00	0.0000E+00	0.0000E+00
8.7740E-06	7.4460E-05	4.7940E-02	5.3972E-01	0.0000E+00	0.0000E+00
0.0000E+00	0.0000E+00	0.0000E+00	0.0000E+00	7.8023E-05	9.2007E-02
5.3829E-01	0.0000E+00	0.0000E+00	0.0000E+00	0.0000E+00	0.0000E+00
0.0000E+00	4.6790E-04	9.8225E-02	4.5754E-01	3.7865E-03	0.0000E+00
0.0000E+00	0.0000E+00	0.0000E+00	2.0669E-05	6.0170E-03	1.2116E-01
4.7705E-01	3.4859E-02	0.0000E+00	0.0000E+00	0.0000E+00	0.0000E+00
7.6756E-04	5.1538E-03	6.1960E-02	4.7171E-01		

Absorber

2.5466E-03	5.6983E-03	2.3329E-02	1.3177E-01	6.5859E-01	2.7791E+00
5.1754E+00	1.1825E+01	0.0000E+00	0.0000E+00	0.0000E+00	0.0000E+00
0.0000E+00	0.0000E+00	0.0000E+00	0.0000E+00	0.0000E+00	0.0000E+00
0.0000E+00	0.0000E+00	0.0000E+00	0.0000E+00	0.0000E+00	0.0000E+00

0.0000E+00	0.0000E+00	0.0000E+00	0.0000E+00	0.0000E+00	0.0000E+00
0.0000E+00	0.0000E+00	1.2788E-01	0.0000E+00	0.0000E+00	0.0000E+00
0.0000E+00	0.0000E+00	0.0000E+00	0.0000E+00	5.6921E-02	2.3506E-01
0.0000E+00	0.0000E+00	0.0000E+00	0.0000E+00	0.0000E+00	0.0000E+00
3.0017E-02	5.2780E-02	3.6613E-01	0.0000E+00	0.0000E+00	0.0000E+00
0.0000E+00	0.0000E+00	1.0522E-06	4.6714E-05	9.5059E-04	3.9343E-01
0.0000E+00	0.0000E+00	0.0000E+00	0.0000E+00	0.0000E+00	2.8836E-06
0.0000E+00	1.4012E-03	3.2955E-01	0.0000E+00	0.0000E+00	0.0000E+00
0.0000E+00	0.0000E+00	0.0000E+00	0.0000E+00	5.5941E-04	2.0981E-01
3.4896E-03	0.0000E+00	0.0000E+00	0.0000E+00	0.0000E+00	0.0000E+00
0.0000E+00	4.8754E-03	2.5351E-01	7.4846E-03	0.0000E+00	0.0000E+00
0.0000E+00	0.0000E+00	0.0000E+00	0.0000E+00	4.0153E-03	2.5385E-01
6.7087E-02	0.0000E+00	0.0000E+00	0.0000E+00	0.0000E+00	0.0000E+00
0.0000E+00	0.0000E+00	0.0000E+00	1.1017E-01	0.0000E+00	0.0000E+00
0.0000E+00	0.0000E+00	0.0000E+00	0.0000E+00	0.0000E+00	0.0000E+00
7.7282E-02	0.0000E+00	0.0000E+00	0.0000E+00	0.0000E+00	0.0000E+00
0.0000E+00	0.0000E+00	0.0000E+00	3.4601E-03	0.0000E+00	0.0000E+00
0.0000E+00	0.0000E+00	0.0000E+00	0.0000E+00	0.0000E+00	0.0000E+00
2.0505E-03	0.0000E+00	0.0000E+00	0.0000E+00	0.0000E+00	0.0000E+00
0.0000E+00	0.0000E+00	0.0000E+00	1.5551E-03	0.0000E+00	0.0000E+00
0.0000E+00	0.0000E+00	0.0000E+00	0.0000E+00	0.0000E+00	0.0000E+00
2.0408E-03	0.0000E+00	0.0000E+00	0.0000E+00	0.0000E+00	0.0000E+00
0.0000E+00	0.0000E+00	0.0000E+00	1.9413E-03		

Gadded Assembly Cross Sections

The following are the cross sections for the gadded EPR assembly. Cross sections are provided for the five unique regions namely, the UO₂ fuel, the zirconium cladding, the moderator, the fuel with 2 wt% gadolinium, and the fuel with 8 wt% gadolinium.

2 Group Cross Sections

Fuel

2.9935E-02	2.8411E-01	9.3329E-03	2.1631E-01	2.5399E+00	2.4338E+00
1.0000E+00	0.0000E+00	3.9496E-01	2.0752E-03	8.2126E-04	4.0514E-01
4.4766E-02	-1.9043E-04	-1.9064E-04	8.9092E-03		

Cladding

1.7460E-03	4.0343E-03	0.0000E+00	0.0000E+00	0.0000E+00	0.0000E+00
0.0000E+00	0.0000E+00	3.1381E-01	9.1070E-04	2.9031E-04	2.7433E-01
3.8257E-02	-1.1260E-04	-6.8211E-05	2.5593E-03		

Moderator

6.6739E-04	2.3325E-02	0.0000E+00	0.0000E+00	0.0000E+00	0.0000E+00
0.0000E+00	0.0000E+00	6.0439E-01	2.4896E-03	2.7157E-02	1.7484E+00
3.6004E-01	1.5511E-03	8.0116E-03	5.2086E-01		

2% Gadolinium

3.6388E-02	2.2416E+00	8.3297E-03	1.1956E-01	2.5444E+00	2.4338E+00
1.0000E+00	0.0000E+00	4.0020E-01	4.8076E-03	8.5424E-04	4.1218E-01

4.3913E-02 -4.2817E-04 -1.9812E-04 9.3425E-03

8% Gadolinium

5.0278E-02 4.5416E+00 6.4369E-03 7.2908E-02 2.5652E+00 2.4338E+00

1.0000E+00 0.0000E+00 4.0692E-01 7.7169E-03 8.1456E-04 4.2652E-01

4.4443E-02 -6.3128E-04 -1.8861E-04 9.7278E-03

4 Group Cross Sections

Fuel

8.4574E-03 8.1334E-02 4.9501E-02 2.8411E-01 4.8820E-03 1.6619E-02

3.0073E-02 2.1631E-01 2.7311E+00 2.4338E+00 2.4338E+00 2.4338E+00

9.9980E-01 1.9568E-04 0.0000E+00 0.0000E+00 3.5465E-01 0.0000E+00

0.0000E+00 0.0000E+00 1.5795E-03 4.9556E-01 0.0000E+00 0.0000E+00

0.0000E+00 2.4250E-03 3.7851E-01 2.0752E-03 0.0000E+00 0.0000E+00

1.5391E-02 4.0514E-01 6.1897E-02 0.0000E+00 0.0000E+00 0.0000E+00

-4.8470E-04 9.1416E-03 0.0000E+00 0.0000E+00 0.0000E+00 -7.3527E-04

1.2268E-02 -1.9043E-04 0.0000E+00 0.0000E+00 -3.5728E-03 8.9092E-03

Cladding

5.7620E-04 4.7178E-03 1.0505E-03 4.0343E-03 0.0000E+00 0.0000E+00

0.0000E+00 0.0000E+00 0.0000E+00 0.0000E+00 0.0000E+00 0.0000E+00

0.0000E+00 0.0000E+00 0.0000E+00 0.0000E+00 3.0968E-01 0.0000E+00

0.0000E+00 0.0000E+00 5.4241E-04 3.3085E-01 0.0000E+00 0.0000E+00

0.0000E+00 6.2477E-04 2.6884E-01 9.1070E-04 0.0000E+00 0.0000E+00

5.2717E-03 2.7433E-01 5.6036E-02 0.0000E+00 0.0000E+00 0.0000E+00

-1.3816E-04	2.6487E-03	0.0000E+00	0.0000E+00	0.0000E+00	-2.0518E-04
3.6318E-03	-1.1260E-04	0.0000E+00	0.0000E+00	-1.2386E-03	2.5593E-03

Moderator

1.5642E-04	7.9835E-04	6.0124E-03	2.3325E-02	0.0000E+00	0.0000E+00
0.0000E+00	0.0000E+00	0.0000E+00	0.0000E+00	0.0000E+00	0.0000E+00
0.0000E+00	0.0000E+00	0.0000E+00	0.0000E+00	3.5633E-01	0.0000E+00
0.0000E+00	0.0000E+00	6.1693E-02	9.3803E-01	0.0000E+00	0.0000E+00
1.9689E-05	8.5477E-02	6.8347E-01	2.4896E-03	1.3027E-06	1.5945E-02
4.0275E-01	1.7484E+00	2.0767E-01	0.0000E+00	0.0000E+00	0.0000E+00
2.6972E-02	5.9355E-01	0.0000E+00	0.0000E+00	0.0000E+00	4.0291E-02
4.5475E-01	1.5511E-03	0.0000E+00	2.7763E-03	1.2853E-01	5.2086E-01

2% Gadolinium

8.3134E-03	9.1621E-02	1.0293E-01	2.2416E+00	4.5531E-03	1.4100E-02
2.5588E-02	1.1956E-01	2.7355E+00	2.4338E+00	2.4338E+00	2.4338E+00
9.9980E-01	1.9630E-04	0.0000E+00	0.0000E+00	3.5802E-01	0.0000E+00
0.0000E+00	0.0000E+00	1.6629E-03	5.0109E-01	0.0000E+00	0.0000E+00
0.0000E+00	2.4716E-03	3.7785E-01	4.8076E-03	0.0000E+00	0.0000E+00
1.5568E-02	4.1218E-01	6.1533E-02	0.0000E+00	0.0000E+00	0.0000E+00
-5.0745E-04	9.2034E-03	0.0000E+00	0.0000E+00	0.0000E+00	-7.4886E-04
1.2331E-02	-4.2817E-04	0.0000E+00	0.0000E+00	-3.6106E-03	9.3425E-03

8% Gadolinium

8.1867E-03	1.1882E-01	2.3423E-01	4.5416E+00	4.0374E-03	1.0027E-02
------------	------------	------------	------------	------------	------------

1.8608E-02	7.2908E-02	2.7449E+00	2.4338E+00	2.4338E+00	2.4338E+00
9.9980E-01	1.9764E-04	0.0000E+00	0.0000E+00	3.6311E-01	0.0000E+00
0.0000E+00	0.0000E+00	1.7117E-03	5.1337E-01	0.0000E+00	0.0000E+00
0.0000E+00	2.5045E-03	3.7613E-01	7.7169E-03	0.0000E+00	0.0000E+00
1.5758E-02	4.2652E-01	6.2047E-02	0.0000E+00	0.0000E+00	0.0000E+00
-5.1347E-04	9.3415E-03	0.0000E+00	0.0000E+00	0.0000E+00	-7.5554E-04
1.2438E-02	-6.3128E-04	0.0000E+00	0.0000E+00	-3.6488E-03	9.7278E-03

8 Group Cross Sections

Fuel

1.4561E-02	8.1946E-03	6.4807E-03	3.8703E-02	1.5089E-01	4.9501E-02
1.7423E-01	3.8033E-01	1.3541E-02	6.2334E-03	1.2657E-03	8.0483E-03
3.0603E-02	3.0073E-02	1.3009E-01	2.9181E-01	2.8822E+00	2.6120E+00
2.4509E+00	2.4338E+00	2.4338E+00	2.4338E+00	2.4338E+00	2.4338E+00
3.5053E-01	4.1072E-01	2.3856E-01	1.9568E-04	0.0000E+00	0.0000E+00
0.0000E+00	0.0000E+00	1.7495E-01	0.0000E+00	0.0000E+00	0.0000E+00
0.0000E+00	0.0000E+00	0.0000E+00	0.0000E+00	3.6064E-02	2.3745E-01
0.0000E+00	0.0000E+00	0.0000E+00	0.0000E+00	0.0000E+00	0.0000E+00
2.2579E-02	5.8674E-02	4.2387E-01	0.0000E+00	0.0000E+00	0.0000E+00
0.0000E+00	0.0000E+00	9.3513E-06	7.1093E-06	2.8605E-03	5.0978E-01
0.0000E+00	0.0000E+00	0.0000E+00	0.0000E+00	2.9879E-25	0.0000E+00
2.1394E-25	5.2373E-03	4.6379E-01	0.0000E+00	0.0000E+00	0.0000E+00
0.0000E+00	0.0000E+00	0.0000E+00	0.0000E+00	6.3814E-03	3.7851E-01
4.4447E-03	0.0000E+00	0.0000E+00	0.0000E+00	0.0000E+00	0.0000E+00
0.0000E+00	1.5391E-02	3.6757E-01	2.8893E-02	0.0000E+00	0.0000E+00

0.0000E+00	0.0000E+00	0.0000E+00	0.0000E+00	3.0609E-02	3.8231E-01
9.7388E-02	0.0000E+00	0.0000E+00	0.0000E+00	0.0000E+00	0.0000E+00
0.0000E+00	0.0000E+00	-3.8457E-04	7.3069E-02	0.0000E+00	0.0000E+00
0.0000E+00	0.0000E+00	0.0000E+00	0.0000E+00	2.9533E-04	-1.0557E-02
4.9425E-02	0.0000E+00	0.0000E+00	0.0000E+00	0.0000E+00	0.0000E+00
3.9858E-07	0.0000E+00	-8.7993E-04	1.0013E-02	0.0000E+00	0.0000E+00
0.0000E+00	0.0000E+00	0.0000E+00	0.0000E+00	0.0000E+00	-1.6059E-03
1.0339E-02	0.0000E+00	0.0000E+00	0.0000E+00	0.0000E+00	0.0000E+00
0.0000E+00	0.0000E+00	-1.9349E-03	1.2268E-02	-4.0787E-04	0.0000E+00
0.0000E+00	0.0000E+00	0.0000E+00	0.0000E+00	0.0000E+00	-3.5726E-03
1.4220E-02	-4.8527E-03	0.0000E+00	0.0000E+00	0.0000E+00	0.0000E+00
0.0000E+00	-2.7475E-07	-4.9898E-03	1.3480E-02		

Cladding

7.9668E-05	4.9487E-04	7.8037E-04	7.5481E-03	2.6944E-04	1.0505E-03
2.4764E-03	5.3248E-03	0.0000E+00	0.0000E+00	0.0000E+00	0.0000E+00
0.0000E+00	0.0000E+00	0.0000E+00	0.0000E+00	0.0000E+00	0.0000E+00
0.0000E+00	0.0000E+00	0.0000E+00	0.0000E+00	0.0000E+00	0.0000E+00
0.0000E+00	0.0000E+00	0.0000E+00	0.0000E+00	0.0000E+00	0.0000E+00
0.0000E+00	0.0000E+00	1.1833E-01	0.0000E+00	0.0000E+00	0.0000E+00
0.0000E+00	0.0000E+00	0.0000E+00	0.0000E+00	3.4600E-02	2.2797E-01
0.0000E+00	0.0000E+00	0.0000E+00	0.0000E+00	0.0000E+00	0.0000E+00
2.0529E-02	1.5877E-02	3.8568E-01	0.0000E+00	0.0000E+00	0.0000E+00
0.0000E+00	0.0000E+00	3.1364E-07	0.0000E+00	9.7367E-04	3.6856E-01
0.0000E+00	0.0000E+00	0.0000E+00	0.0000E+00	0.0000E+00	0.0000E+00

0.0000E+00	1.2550E-03	2.6962E-01	0.0000E+00	0.0000E+00	0.0000E+00
0.0000E+00	0.0000E+00	0.0000E+00	0.0000E+00	1.6067E-03	2.6884E-01
2.0101E-03	0.0000E+00	0.0000E+00	0.0000E+00	0.0000E+00	0.0000E+00
0.0000E+00	5.2717E-03	2.5912E-01	9.6948E-03	0.0000E+00	0.0000E+00
0.0000E+00	0.0000E+00	0.0000E+00	0.0000E+00	1.3359E-02	2.6617E-01
5.3508E-02	0.0000E+00	0.0000E+00	0.0000E+00	0.0000E+00	0.0000E+00
0.0000E+00	0.0000E+00	-4.7662E-04	7.9676E-02	0.0000E+00	0.0000E+00
0.0000E+00	0.0000E+00	0.0000E+00	0.0000E+00	-1.2404E-05	-7.2483E-04
4.6523E-02	0.0000E+00	0.0000E+00	0.0000E+00	0.0000E+00	0.0000E+00
0.0000E+00	0.0000E+00	-2.4804E-04	3.1382E-03	0.0000E+00	0.0000E+00
0.0000E+00	0.0000E+00	0.0000E+00	0.0000E+00	0.0000E+00	-4.1205E-04
2.5270E-03	0.0000E+00	0.0000E+00	0.0000E+00	0.0000E+00	0.0000E+00
0.0000E+00	0.0000E+00	-5.2765E-04	3.6318E-03	-2.4852E-04	0.0000E+00
0.0000E+00	0.0000E+00	0.0000E+00	0.0000E+00	0.0000E+00	-1.2386E-03
5.3237E-03	-1.7500E-03	0.0000E+00	0.0000E+00	0.0000E+00	0.0000E+00
0.0000E+00	0.0000E+00	-2.5604E-03	4.1404E-03		

Moderator

7.7294E-04	4.2546E-06	1.9972E-05	2.5266E-04	1.6399E-03	6.0124E-03
1.4122E-02	3.0652E-02	0.0000E+00	0.0000E+00	0.0000E+00	0.0000E+00
0.0000E+00	0.0000E+00	0.0000E+00	0.0000E+00	0.0000E+00	0.0000E+00
0.0000E+00	0.0000E+00	0.0000E+00	0.0000E+00	0.0000E+00	0.0000E+00
0.0000E+00	0.0000E+00	0.0000E+00	0.0000E+00	0.0000E+00	0.0000E+00
0.0000E+00	0.0000E+00	5.8861E-02	0.0000E+00	0.0000E+00	0.0000E+00
0.0000E+00	0.0000E+00	0.0000E+00	0.0000E+00	4.8447E-02	1.1709E-01

0.0000E+00	0.0000E+00	0.0000E+00	0.0000E+00	0.0000E+00	0.0000E+00
2.6438E-02	1.2268E-01	4.8318E-01	0.0000E+00	0.0000E+00	0.0000E+00
0.0000E+00	0.0000E+00	2.9114E-04	1.2292E-03	1.0800E-01	8.2002E-01
0.0000E+00	0.0000E+00	0.0000E+00	0.0000E+00	0.0000E+00	9.8554E-06
1.4939E-03	2.0658E-01	8.0146E-01	0.0000E+00	0.0000E+00	0.0000E+00
0.0000E+00	0.0000E+00	3.5153E-05	5.3461E-03	2.0905E-01	6.8347E-01
5.6165E-03	0.0000E+00	0.0000E+00	0.0000E+00	2.3259E-06	7.7557E-04
2.9927E-02	3.3451E-01	8.9634E-01	1.8999E-01	0.0000E+00	0.0000E+00
0.0000E+00	2.1446E-04	9.0803E-03	6.8239E-02	4.4834E-01	1.8798E+00
3.3534E-02	0.0000E+00	0.0000E+00	0.0000E+00	0.0000E+00	0.0000E+00
0.0000E+00	0.0000E+00	3.1482E-02	6.3933E-02	0.0000E+00	0.0000E+00
0.0000E+00	0.0000E+00	0.0000E+00	0.0000E+00	9.3984E-03	5.6536E-02
2.9150E-01	0.0000E+00	0.0000E+00	0.0000E+00	0.0000E+00	0.0000E+00
8.7370E-06	7.4091E-05	4.8042E-02	5.3893E-01	0.0000E+00	0.0000E+00
0.0000E+00	0.0000E+00	0.0000E+00	0.0000E+00	7.8214E-05	9.2844E-02
5.3460E-01	0.0000E+00	0.0000E+00	0.0000E+00	0.0000E+00	0.0000E+00
0.0000E+00	4.7230E-04	1.0170E-01	4.5475E-01	3.4993E-03	0.0000E+00
0.0000E+00	0.0000E+00	0.0000E+00	2.0907E-05	6.2302E-03	1.2333E-01
4.7469E-01	3.4365E-02	0.0000E+00	0.0000E+00	0.0000E+00	0.0000E+00
7.9543E-04	5.2007E-03	6.4461E-02	4.7192E-01		

2% Gadolinium

1.4238E-02	7.9802E-03	6.5162E-03	4.3952E-02	1.6878E-01	1.0293E-01
7.6685E-01	8.8339E+00	1.3197E-02	5.9774E-03	1.0697E-03	6.7736E-03
2.5960E-02	2.5588E-02	1.0339E-01	1.9185E-01	2.8821E+00	2.6127E+00

2.4506E+00	2.4338E+00	2.4338E+00	2.4338E+00	2.4338E+00	2.4338E+00
3.5053E-01	4.1065E-01	2.3862E-01	1.9630E-04	0.0000E+00	0.0000E+00
0.0000E+00	0.0000E+00	1.7495E-01	0.0000E+00	0.0000E+00	0.0000E+00
0.0000E+00	0.0000E+00	0.0000E+00	0.0000E+00	3.6433E-02	2.3924E-01
0.0000E+00	0.0000E+00	0.0000E+00	0.0000E+00	0.0000E+00	0.0000E+00
2.2810E-02	5.9097E-02	4.2563E-01	0.0000E+00	0.0000E+00	0.0000E+00
0.0000E+00	0.0000E+00	9.0826E-06	7.8939E-06	2.9523E-03	5.1824E-01
0.0000E+00	0.0000E+00	0.0000E+00	0.0000E+00	2.9962E-25	0.0000E+00
2.1008E-25	5.2778E-03	4.6479E-01	0.0000E+00	0.0000E+00	0.0000E+00
0.0000E+00	0.0000E+00	0.0000E+00	0.0000E+00	6.4724E-03	3.7785E-01
5.8831E-03	0.0000E+00	0.0000E+00	0.0000E+00	0.0000E+00	0.0000E+00
0.0000E+00	1.5568E-02	3.8055E-01	5.2223E-02	0.0000E+00	0.0000E+00
0.0000E+00	0.0000E+00	0.0000E+00	0.0000E+00	2.1526E-02	4.0515E-01
9.7524E-02	0.0000E+00	0.0000E+00	0.0000E+00	0.0000E+00	0.0000E+00
0.0000E+00	0.0000E+00	-4.2171E-04	7.4005E-02	0.0000E+00	0.0000E+00
0.0000E+00	0.0000E+00	0.0000E+00	0.0000E+00	2.9068E-04	-1.0613E-02
4.8906E-02	0.0000E+00	0.0000E+00	0.0000E+00	0.0000E+00	0.0000E+00
3.9370E-07	0.0000E+00	-9.0308E-04	1.0079E-02	0.0000E+00	0.0000E+00
0.0000E+00	0.0000E+00	0.0000E+00	0.0000E+00	0.0000E+00	-1.6107E-03
1.0394E-02	0.0000E+00	0.0000E+00	0.0000E+00	0.0000E+00	0.0000E+00
0.0000E+00	0.0000E+00	-1.9611E-03	1.2331E-02	-5.2395E-04	0.0000E+00
0.0000E+00	0.0000E+00	0.0000E+00	0.0000E+00	0.0000E+00	-3.6104E-03
1.3302E-02	-6.6265E-03	0.0000E+00	0.0000E+00	0.0000E+00	0.0000E+00
0.0000E+00	-2.7733E-07	-3.8995E-03	1.5701E-02		

8% Gadolinium

1.3391E-02	7.5658E-03	6.7888E-03	6.0340E-02	2.1549E-01	2.3423E-01
1.8954E+00	3.3247E+01	1.2286E-02	5.4415E-03	7.6340E-04	4.7957E-03
1.8675E-02	1.8608E-02	6.7232E-02	1.3448E-01	2.8818E+00	2.6138E+00
2.4508E+00	2.4338E+00	2.4338E+00	2.4338E+00	2.4338E+00	2.4338E+00
3.5055E-01	4.1050E-01	2.3875E-01	1.9764E-04	0.0000E+00	0.0000E+00
0.0000E+00	0.0000E+00	1.7630E-01	0.0000E+00	0.0000E+00	0.0000E+00
0.0000E+00	0.0000E+00	0.0000E+00	0.0000E+00	3.7259E-02	2.4458E-01
0.0000E+00	0.0000E+00	0.0000E+00	0.0000E+00	0.0000E+00	0.0000E+00
2.3470E-02	6.0104E-02	4.2953E-01	0.0000E+00	0.0000E+00	0.0000E+00
0.0000E+00	0.0000E+00	8.4805E-06	1.0504E-05	3.0132E-03	5.3800E-01
0.0000E+00	0.0000E+00	0.0000E+00	0.0000E+00	2.9893E-25	0.0000E+00
2.0880E-25	5.2737E-03	4.6393E-01	0.0000E+00	0.0000E+00	0.0000E+00
0.0000E+00	0.0000E+00	0.0000E+00	0.0000E+00	6.6444E-03	3.7613E-01
8.4282E-03	0.0000E+00	0.0000E+00	0.0000E+00	0.0000E+00	0.0000E+00
0.0000E+00	1.5758E-02	3.9663E-01	6.1103E-02	0.0000E+00	0.0000E+00
0.0000E+00	0.0000E+00	0.0000E+00	0.0000E+00	1.3641E-02	5.4165E-01
9.8406E-02	0.0000E+00	0.0000E+00	0.0000E+00	0.0000E+00	0.0000E+00
0.0000E+00	0.0000E+00	-5.0934E-04	7.6798E-02	0.0000E+00	0.0000E+00
0.0000E+00	0.0000E+00	0.0000E+00	0.0000E+00	2.7430E-04	-1.0770E-02
4.8670E-02	0.0000E+00	0.0000E+00	0.0000E+00	0.0000E+00	0.0000E+00
3.7252E-07	0.0000E+00	-9.0624E-04	1.0224E-02	0.0000E+00	0.0000E+00
0.0000E+00	0.0000E+00	0.0000E+00	0.0000E+00	0.0000E+00	-1.5881E-03
1.0508E-02	0.0000E+00	0.0000E+00	0.0000E+00	0.0000E+00	0.0000E+00
0.0000E+00	0.0000E+00	-2.0044E-03	1.2438E-02	-6.8948E-04	0.0000E+00

0.0000E+00	0.0000E+00	0.0000E+00	0.0000E+00	0.0000E+00	-3.6485E-03
1.2366E-02	-6.5896E-03	0.0000E+00	0.0000E+00	0.0000E+00	0.0000E+00
0.0000E+00	-2.7853E-07	-2.6576E-03	1.6532E-02		

REFERENCES

- [1] K. Smith, "Assembly Homogenization techniques for Light Water Reactor Analysis." *Progress in Nuclear Energy*, 17, 303-335 (1986).
- [2] S. Mosher and F. Rahnema, "The Incident Flux Response Expansion Method for Heterogeneous Coarse Mesh Transport Problems," *Transport Theory and Statistical Physics*, 35, No. 1, 55-86 (2006).
- [3] D. Zhang and F. Rahnema, "An Efficient Hybrid Stochastic/Deterministic Coarse Mesh Neutron Transport Method," *Annals of Nuclear Energy*, 41, 1-11 (2012).
- [4] K. Connolly and F. Rahnema, "Heterogeneous Coarse Mesh Radiation Transport Method for Neutronic Analysis of Prismatic Reactors," *Annals of Nuclear Energy*, 56, 87-101 (2013).
- [5] D. Zhang and F. Rahnema, "A Whole-Core Coarse Mesh Neutron Transport Method in 2-D Cylindrical (R, Theta) Geometry," *Nucl. Eng. Des.*, 265, 997-1004 (2013).
- [6] Pelowitz, D. B., et al., *MCNP6 user's manual version 1.0*. LA-CP-13-00634. Los Alamos, NM: Los Alamos National Laboratory (2013).
- [7] D. Zhang and F. Rahnema, "High-Order Perturbation Theory for Incident Flux Response Expansion Methods," *Nuclear Science and Engineering*, 176, 69-80 (2014).
- [8] D. Zhang and F. Rahnema, "A fission collision separation method for efficient incident flux response expansion coefficient generation," *Annals of Nuclear Energy*, 73, 264-269 (2014).
- [9] D. Zhang and F. Rahnema, "An Efficient Hybrid Stochastic/Deterministic Coarse Mesh Neutron Transport Method," *Annals of Nuclear Energy*, 41, 1-11 (2012).
- [10] S. Dupree and S. Fraley, "A Monte Carlo Primer, A Practical Approach to Radiation Transport," Kluwer Academic / Plenum Publishers, New York. (2002).
- [11] M. B. Emmett, "The MORSE Monte Carlo Radiation Transport Code System," ORNL-4972, Oak Ridge, TN: Union Carbide Corp. Oak Ridge National Laboratory. (1975).
- [12] J. C. Wagner et al., "MCNP: Multigroup/Adjoint Capabilities," LA-12704, Los Alamos, NM. Los Alamos National Laboratory. (1994).

- [13] M. B. Chadwick, et al., "ENDF/B-VII.1: Nuclear Data for Science and Technology: Cross Sections, Covariances, Fission Product Yields and Decay Data", Nucl. Data Sheets 112 (2011).
- [14] R. E. MacFarlane and R. M. Boicourt, "NJOY: A Neutron and Photon Processing System," Trans. Am. Nucl. Soc. 22, 720 (1975).
- [15] M. E. Dunn and N. M. Greene, "AMPX-2000: A Cross-Section Processing System for Generating Nuclear Data for Criticality Safety Applications," Trans. Am. Nucl. Soc. 86, 118-119 (2002).
- [16] A. Haghghat, "Monte Carlo Methods for Particle Transport," CRC Press, Boca Raton. (2015).
- [17] AREVA. U.S. EPR Final Safety Analysis Report - AREVA Design Control Document Rev. 5 (2013).
- [18] T. Simeonov, "Release Notes – Helios System Version 1.8," Studsvik Scandpower Report, SSP-03/221 (2003).

VITA

Ryan Hon was born in 1989 in Rockaway, New Jersey to Lynne and Sam Hon. He grew up there with his younger sister Alyssa before his father's job took the family to Melbourne, Australia in 1999. Having enjoyed the Australian culture for two years, the family then moved to Atlanta, Georgia. Ryan spent his high school years at Northview, graduating in 2007, and then attended the Georgia Institute of Technology. There he earned two degrees, a Bachelor of Science in Nuclear and Radiological Engineering in 2011 and a Master of Science in Nuclear Engineering. Ryan currently lives in Atlanta with his wife Kelly. He hopes to hike the Appalachian Trail before settling down with his wife and starting a family.